New pharmacodynamic parameters linked with ibrutinib responses in chronic lymphocytic leukemia: Prospective study in real-world patients and mathematical modeling

Sarah Cadot, Chloe Audebert, Charlotte Dion, Soleakhena Ken, Loic Dupré, Laetitia Largeaud, Camille Laurent, Loic Ysebaert, Fabien Crauste, Anne Quillet-Mary

PLOS MEDICINE

RESEARCH ARTICLE

New pharmacodynamic parameters linked with ibrutinib responses in chronic lymphocytic leukemia: Prospective study in real-world patients and mathematical modeling

Sarah Cadot[1,2☯], Chloe Audebert[3,4☯], Charlotte Dion[5], Soleakhena Ken[1,6], Loic Dupré[7,8], Laetitia Largeaud[1,9], Camille Laurent[1,2,9], Loic Ysebaert[1,2,9], Fabien Crauste[10☯], Anne Quillet-Mary[1,2☯]*

1 INSERM UMR1037, CNRS UMR5071, Université Toulouse III-Paul Sabatier, Centre de Recherches en Cancérologie de Toulouse, Toulouse, France, **2** Laboratoire d'Excellence 'TOUCAN-2', Toulouse, France, **3** Sorbonne Université, CNRS, Université Paris Cité, Laboratoire Jacques-Louis Lions UMR 7598, Paris, France, **4** Sorbonne Université, CNRS, Institut de Biologie Paris-Seine, Laboratoire de Biologie Computationnelle et Quantitative UMR 7238, Paris, France, **5** Sorbonne Université, UMR CNRS 8001, LPSM, Paris, France, **6** Institut Claudius Regaud- Institut Universitaire du Cancer de Toulouse-Oncopole, Toulouse, France, **7** Institut Toulousain des Maladies Infectieuses et Inflammatoires, INSERM, CNRS, Université Toulouse III-Paul Sabatier, Toulouse, France, **8** Department of Dermatology, Medical University of Vienna, Vienna, Austria, **9** Institut Universitaire du Cancer-Oncopole de Toulouse, Toulouse, France, **10** Université Paris Cité, CNRS, MAP5 UMR 8145, Paris, France

☯ These authors contributed equally to this work.
* anne.quillet-mary@inserm.fr

Citation: Cadot S, Audebert C, Dion C, Ken S, Dupré L, Largeaud L, et al. (2024) New pharmacodynamic parameters linked with ibrutinib responses in chronic lymphocytic leukemia: Prospective study in real-world patients and mathematical modeling. PLoS Med 21(7): e1004430. https://doi.org/10.1371/journal.pmed.1004430

Academic Editor: Aadel A. Chaudhuri, Washington University in St Louis, UNITED STATES OF AMERICA

Received: July 27, 2023

Accepted: June 19, 2024

Published: July 22, 2024

Data Availability Statement: All relevant data are within the manuscript and its Supporting Information files.

Funding: This work was supported by Institut National du Cancer within the framework of C15093BS-Cancer Plan (SC, SK, LD, LY, AQM); Agence Nationale de la Recherche within the framework of LABEX-TOUCAN (SC, CL, LY, AQM);

Abstract

Background

One of the first clinical observations of ibrutinib activity in the treatment of chronic lymphocytic leukemia (CLL) is a rapid decline in lymph nodes size. This phenomenon is accompanied by an hyperlymphocytosis, either transient or prolonged, which is associated with distinct clinical responses and thus has an impact on long-term outcomes. Understanding which factors determine distinct disease courses upon ibrutinib treatment remains a scientific challenge.

Methods and findings

From 2016 to 2021, we conducted a longitudinal and observational study in 2 cohorts of patients with chronic lymphocytic leukemia (CLL) (cohort 1, $n = 41$; cohort 2, $n = 81$). These cohorts reflect the well-known clinical features of CLL patients, such as Male/Female sex ratio of 2/1, a median age of 70 years at diagnosis, and include patients in first-line therapy (27%) or relapsed/refractory patients (73%). Blood cell counts were followed for each patient during 2 years of ibrutinib treatment. In addition, immunophenotyping and whole-body magnetic resonance imaging (MRI) were assessed in patients from cohort 1. These data were integrated in a newly built mathematical model, inspired by previous

Centre National de la Recherche Scientifique within the framework of EDYLE (SC, CA, CD, LD, LY, FC, AQM); La Ligue contre le Cancer, within the framework of Comites 11,32,65 (LY, AQM). The funders of the study have no role in study design, data collection, data analysis, data interpretation, preparation or writing the report.

Competing interests: The authors have declared that no competing interests exist.

Abbreviations: ADC, apparent diffusion coefficient; ALC, absolute lymphocyte count; CLL, chronic lymphocytic leukemia; ITK, interleukin-2-inducible T-cell kinase; LN, lymph node; MRI, magnetic resonance imaging; NLME, nonlinear mixed effect; ODE, ordinary differential equation; OS, overall survival; PBMC, peripheral blood mononuclear cell; PFS, progression-free survival; pHL, prolonged hyperlymphocytosis; SAMBA, Stochastic Approximation for Model Building Algorithm; tHL, transient hyperlymphocytosis.

mathematical works on CLL treatment and combining dynamical and statistical models, leading to the identification of biological mechanisms associated with the 2 types of clinical responses. This multidisciplinary approach allowed to identify baseline parameters that dictated lymphocytes kinetics upon ibrutinib treatment. Indeed, ibrutinib-induced lymphocytosis defined 2 CLL patient subgroups, transient hyperlymphocytosis (tHL) or prolonged hyperlymphocytosis (pHL), that can be discriminated, before the treatment, by absolute counts of $CD4^+$ T lymphocytes ($p = 0.026$) and regulatory CD4 T cells ($p = 0.007$), programmed cell death protein 1 PD1 ($p = 0.022$) and CD69 ($p = 0.03$) expression on B leukemic cells, CD19/$CD5^{high}$/$CXCR4^{low}$ level ($p = 0.04$), and lymph node cellularity. We also pinpointed that the group of patients identified by the transient hyperlymphocytosis has lower duration response and a poor clinical outcome. The mathematical approach led to the reproduction of patient-specific dynamics and the estimation of associated patient-specific biological parameters, and highlighted that the differences between the 2 groups were mainly due to the production of leukemic B cells in lymph node compartments, and to a lesser extent to T lymphocytes and leukemic B cell egress into bloodstream. Access to additional data, especially longitudinal MRI data, could strengthen the conclusions regarding leukemic B cell dynamics in lymph nodes and the relevance of 2 distinct groups of patients.

Conclusions

Altogether, our multidisciplinary study provides a better understanding of ibrutinib response and highlights new pharmacodynamic parameters before and along ibrutinib treatment. Since our results highlight a reduced duration response and outcome in patients with transient hyperlymphocytosis, our approach provides support for managing ibrutinib therapy after 3 months of treatment.

Trial registration

ClinicalTrials.gov NCT02824159.

Author summary

Why was this study done?

- Treatment of chronic lymphocytic leukemia (CLL) was revolutionized by the introduction of targeted therapies such as ibrutinib. Previous studies showed that lymphocyte kinetics under ibrutinib treatment are related to clinical outcome, but some potential mechanisms underlying these responses have not been fully explored.
- This study was done to decipher key biological and pharmacodynamic factors involved in ibrutinib response.

What did the researchers do and find?

- Relying on a cohort of patients treated with ibrutinib, we combined clinical parameters, biological monitoring, whole-body tissue imaging, and mathematical modeling to

decipher key biological and pharmacodynamic factors underlying the 2 distinct groups of ibrutinib response, transient or prolonged hyperlymphocytosis.

- We elaborated a mathematical model, based on previous ones of CLL and combining both dynamical and statistical approaches, that characterizes inter-patient variability and estimates patient-specific biological parameters associated with the 2 groups of response.
- We identified clinical factors (age, absolute lymphocyte counts) and biological factors, such as absolute counts of $CD4^+$ T lymphocytes and regulatory CD4 T cells, programmed cell death protein 1 and CD69 expression on B leukemic cells, $CD19/CD5^{high}/CXCR4^{low}$ level in blood, and lymph node cellularity, before and during ibrutinib therapy. These biomarkers are predictive of ibrutinib response.
- The mathematical approach confirmed the identified clinical factors, by highlighting that the differences between the 2 types of response to ibrutinib treatment were mainly due to the production of leukemic B cells in lymph node compartments, and to a lesser extent to T lymphocytes and leukemic B cell egress into bloodstream.
- We found that the group of patients identified by the transient hyperlymphocytosis has lower duration response and a poor clinical outcome.

What do these findings means?

- Estimation of patient-specific biological parameters in the mathematical models highlights that only few biological processes are group-specific when CLL patients are treated with ibrutinib.
- Biomarkers defined in this study can be easily monitored in CLL patients before and during ibrutinib treatment.
- These results offer potential support for optimizing the management of ibrutinib treatment, especially in the first months of therapy.
- Access to additional data, especially longitudinal magnetic resonance imaging (MRI) data, could strengthen the conclusions regarding leukemic B cell dynamics in lymph nodes.

Introduction

Management of chronic lymphocytic leukemia (CLL), in first-line and relapsed/refractory settings, has been revolutionized by the introduction of oral, targeted agents against Bruton Tyrosine Kinase (ibrutinib), PI-3Kinase (idelalisib), and Bcl-2 (venetoclax) [1,2]. In real-world practice, ibrutinib has been used since 2014 in relapsed/refractory patients and in first-line patients with TP53 abnormalities. The mechanisms by which ibrutinib targets CLL and restores normal immune subsets include: direct cell killing (mostly in tissues), egress from tissue niches, and inhibition of proliferation by targeting B cell receptor signaling and activation of canonical NF-kB pathway, primarily in the lymph node (LN) tumor microenvironment [3,4]. These effects led to an increase of absolute lymphocyte counts (ALCs) in parallel of efflux from tissue compartments, whose kinetics appears heterogeneous across patients' cohorts [5–8].

Kinetics of lymphocytosis upon ibrutinib treatment has been first described by Wiestner's group [6]. In this Phase 2 study [6], 3 profiles of ALCs were described in which 1 subset showed a long-lasting ALCs increase over time (prolonged hyperlymphocytosis (pHL), linked to lower baseline ALCs, immunoglobulin heavy chain variable region genes mutated status, and bulky disease). Importantly, none of those subsets were found correlated to clinical outcomes. Prolonged hyperlymphocytosis with a slight modification of definition was reported in 69% of RESONATE (relapsed/refractory CLL) and 57% of RESONATE-2 (first-line CLL without deletion 17p) patients respectively, but this time was found to be correlated with an improvement of progression-free survival (PFS) only in the relapsed/refractory patients after 19 months follow-up [8,9]. It suggested that lack of initial hyperlymphocytosis could be considered as an easy and rapidly assessable risk factor for progressions [8,10].

Besides its efficacy against CLL cells, ibrutinib displays "on-target" and "off-tumor" effects, explaining some of the adverse events [11,12], but might also be responsible for disease-related immune suppression state [13–15]. One of the hallmarks of this disease is indeed a profound immunosuppression due to impairment of T cells proliferation, cytokine production, immune synapse formation, leading to accumulation of exhausted programmed cell death protein 1 ($PD1^+$) T cells, and increase in $CD4^+CD25^{high}CD127^{low}$ regulatory T cells (Tregs) [15]. Under ibrutinib, immuno-monitoring of PD1 levels at the surface of $CD4^+$ and $CD8^+$ T cells have been reported from small cohorts (7, 14, and 17 patients) in 3 independent studies, without correlation to clinical outcomes [16–18]. On the leukemic B cell compartment, ibrutinib treatment has been shown to be associated with a reduction of PD1 expression (more pronounced than on the T cell compartment) [18], the consequences of which remain unknown.

Mathematical modeling contributed to better understand ibrutinib-induced mechanisms in CLL patients [5]. The model introduced by Wodarz and colleagues [5] and later used in Burger and colleagues [7] consisted in 2 ordinary differential equations (ODEs) describing leukemic B cell dynamics in LN/spleen and blood. The authors concluded that ibrutinib mainly affects leukemic B cell death, with larger death rates in tissues than in blood. In 2014, Komarova and colleagues [19] focused on the development of ibrutinib resistance using methods from evolutionary and computational biology. These works impacted the clinical understanding of CLL and have been essential in the development of current CLL treatments.

Here, using a longitudinal and observational study of CLL patients, we investigated clinico-biological and imaging parameters predicting 2 groups of response induced by ibrutinib (ALCs but also specific immunomodulatory effects of ibrutinib). We explored whether these markers could be correlated to each other and/or to duration of treatment response. To do so, we have designed a mathematical model built on our data and previous mathematical models [5,7] and focused on both leukemic B and T cell counts co-evolution. We have elaborated a modeling approach based on the coupling of ODE describing leukemic B and T cell dynamics and nonlinear mixed effect (NLME) modeling. This approach enables to describe observed inter-patient variability. To our knowledge, no NLME model has been studied for CLL under treatment. We combined the results of clinical analyses and mathematical model parameter estimation to identify which effects explain the 2 ibrutinib-induced patterns of lymphocytosis.

Methods and materials

Ethics statement, patients, and treatment

Peripheral blood samples from ibrutinib-treated CLL patient ($n = 122$: cohort 1, $n = 41$; cohort 2, $n = 81$) were obtained from the Hematology Department with written informed consent and referenced in INSERM cell bank. According to French law, INSERM cell bank has been registered with the Ministry of Higher Education and Research (DC-2013-1903). Clinical and biological annotations

of the samples have been reported to the Comité National Informatique et Liberté. This longitudinal and observational study was approved by the competent authority (ANSM, n˚ 1551668A-11), the ethics committee (N˚ CPP16-004a) and registered by Clinical-Trials.gov (NCT02824159).

This study is reported as per the Strengthening the Reporting of Observational studies in Epidemiology (STROBE) guideline (S1 STROBE Checklist).

Immuno-monitoring study design

Among 122 ibrutinib-treated CLL patients included in the protocol, 41 patients were followed for a two-year period from the treatment initiation (M0: Month 0). Peripheral blood samples were collected at different times of the treatment phase (M0, M1, M2, M3, M6, M12, M18, and M24).

Immunofluorescence staining and analysis. For cell surface staining, peripheral blood mononuclear cells (PBMCs) were incubated with conjugated antibodies (S1 Table) in phosphate buffer saline with 1% inactivated fetal calf serum for 20 min at 4˚C in the dark. For intra cellular staining, surface labeled PBMC were fixed for 15 min at room temperature in paraformaldehyde 1.4%, then permeabilized using BD Phosflow Perm Buffer II (BD Bioscience), washed and stained with BTK (Bruton Tyrosine Kinase) and p-BTK conjugated-antibodies for 20 min at 4˚C in the dark. Samples were measured on a BD LSR II cytometer and analyzed with BD FACS Diva software (BD Bioscience).

In vitro blood cell depletion assay. In vitro ibrutinib sensitivity was quantified using B cell depletion assay [20]. Briefly at each time of ibrutinib treatment, fresh PBMC were seeded at 1×10^7 cells/ml in culture medium (providing long-term viability) and treated by relevant doses of ibrutinib for 7 days. $CD19^+/CD5^+$ (B leukemic cells) levels were determined by flow cytometry. B-cell depletion relative to untreated controls was determined by flow cytometry combined with absolute number quantification as previously described [20].

Statistical analyses of medical and biological data. They were done using two-tailed Mann–Whitney test (unpaired samples) or Student *t* test (paired samples).

Lymph nodes segmentations

Whole body anatomic magnetic resonance imaging (MRI) was acquired at baseline (M0) for 26 patients of cohort 1 (who accepted MRI protocol) and consisted on several 3D volume stages of T1 weighted axial images. These patients who have been analyzed with diffusion-weighted MRI study were the same patients analyzed in our previous study [21] except 1 patient whose acquisition encountered problem of image reconstruction. The parameters of the diffusion-weighted MRI are the following: Repetition Time/Echo Time/Inversion Time = 6,930 ms/71 ms/160 ms with 2 b-value of 50 and 800 s/mm^2. Diffusion images were obtained by averaging over 2 acquisitions. The number of stages was adjusted according to patient size to cover the whole body. To reduce motion artifact, volume stages corresponding to thoracic and abdominal regions were acquired in breath holding condition. Cervical, axillary, mediastinal, retroperitoneal, iliac, inguinal, and splenic regions of interest were segmented with a dedicated semiautomatic method [21]. After a clinical validation by 2 radiologists, the lymph nodes segmentations allowed us to compute the volumes (in ml) and to map these regions of interest on the diffusion modality from which the apparent diffusion coefficient (ADC) (mm^2/s) was done for the first 9 patients. ADC is related to cellularity that captures the degree of abnormal cellular packing and density.

Cell count dynamics study and modeling

Among the 122 patients, group classification was defined according to previously described clinical results [8,9] and thus, pHL was defined as having an ALCs at M3 larger than at M0 (ALC M3 > ALC M0).

Based on known interactions between B and T cells, and inspired by Wodarz and colleagues [5] model, a generic model of B and T cell dynamics under ibrutinib treatment was built and validated on medical data to reproduce the behavior of an average patient. The model accounts for clinical observable variables: $CD19^+/CD5^+$ B cell counts in LN (denoted by B_{LN}), and $CD19^+/CD5^+$ B cell (B_{bl}), CD4 T cell (T_4), CD8 T cell (T_8), Natural Killer (NK) cell (T_{NK}), and Regulatory CD4 T cell (T_{regs}) counts in blood. Dynamics of leukemic B cells are described by a model similar to the one in Wodarz and colleagues [5], where cells exit LN with a rate F_{out} and are produced within LN with a constant rate F_{in}. Dynamics of T cells follow a standard equation, including T cell renewal and production from LN. Model's parameters are described in Table 1 and details of the modeling procedure are available in S1 File Modeling.

The model has been validated, in patients with and without pHL, separately by data fitting (mean values of cell counts at M1, M2, M3, M6, M12, M18, and M24 for blood measurements, and M1, M12 an M24 for LN measurements, obtained through volume estimations MRI measurements). Least-squares minimization has been used to optimize parameter values. Parameter value estimation and data fitting have been performed using Data2Dynamics [22,23], a Matlab R2019b add-on (S1 File Modeling), and for each parameter, profile likelihood-based confidence intervals [24] are provided.

Model development and its analysis have been performed following Garnett and colleagues guidelines [25].

Population approach and inter-patient variability

To account for inter-patient variability in the mathematical model, we used a population approach based on mixed-effect modeling [26]. NLME models allow the description of inter-patient variability within a population of individuals by assuming all individuals in the

Table 1. Variables and parameters of the model of B and T cell dynamics. (d–day; LN, lymph nodes; NK, Natural Killer cells; Tregs, regulatory CD4 T cells).

Variables and parameters	*Unit*	*Description*
B_{LN}	cell count	Leukemic B cell count in LN
B_{bl}	cell count	Leukemic B cell count in blood
T_4	cell count	CD4 T cell count in blood
T_8	cell count	CD8 T cell count in blood
T_{NK}	cell count	NK cell count in blood
T_{regs}	cell count	Tregs cell count in blood
B_{LN}^0	cell count	Initial leukemic B cell count in LN
B_{bl}^0	cell count	Initial leukemic B cell count in blood
T_4^0	cell count	Initial CD4 T cell count in blood
T_8^0	cell count	Initial CD8 T cell count in blood
T_{NK}^0	cell count	Initial NK cell count in blood
T_{regs}^0	cell count	Initial Tregs cell count in blood
F_{out}	d^{-1}	Lymph node exit rate
F_{in}	$cell.d^{-1}$	Leukemic B cell lymph node production rate
μ_B	d^{-1}	Leukemic B cell death rate
μ_4	d^{-1}	CD4 T cell death rate
μ_8	d^{-1}	CD8 T cell death rate
μ_{NK}	d^{-1}	NK cell death rate
μ_{reg}	d^{-1}	Tregs death rate
t	d	Time

https://doi.org/10.1371/journal.pmed.1004430.t001

population (here CLL patients) share common characteristics (fixed effects) while each patient is unique and differs from the average behavior by a specific value (random effect) [26–29]. Details are available in S1 File Modeling.

Parameter values were estimated with Stochastic Approximation Expectation-Maximization algorithm [30]. A categorical covariate was used to characterize groups of patients. Clinical cell counts were pooled together, and then parameter values were estimated assuming that fixed effects were different between groups of patients. Estimated covariate parameters were tested to be significantly different from zero with a Wald test implemented in Monolix software [30] and a *p*-value threshold at 0.05 (see S1 File Modeling).

Model selection

The generic model of B and T cell count dynamics has been selected using a procedure of model selection based on data fitting, parameter estimation, and comparison of statistical indicators (corrected Akaike information criterion). All details and tested models are provided in S1 File Modeling.

To describe inter-patient variability, an error model must be assessed for each variable, parameter correlations, and significant covariates must be selected. The Stochastic Approximation for Model Building Algorithm (SAMBA) [31] is an iterative procedure that allows to build a covariate, a correlation, and an error model automatically. The procedure relies on Monolix simulations and uses the corrected Bayesian information criterion to validate its selection.

An appropriate NLME model was selected using the SAMBA implementation in the function *buildmlx* and the variability model (random effects needed to explain the data) was built with *buildVar* function both of the R package Rsmlx [32]. SAMBA does not guarantee that a global minimum will be reached. Consequently, SAMBA was performed with 5 different initial configurations (S2 Table) and the model with all common features was selected. Finally, a multi-start approach available in Monolix [30] was performed to ensure that estimations were robust and the model was practically identifiable.

Results

Ibrutinib-induced lymphocytosis defines 2 CLL patient subgroups

In our 122 patients (S3 Table) treatment-induced lymphocytosis was highly variable between patients (Fig 1A). Yet, we applied the previously described cut-off [8,9] to easily classify patients according to lymphocytosis status, irrespectively of percent ALC rise: tHL group (transient hyperlymphocytosis) had short-lived lymphocytosis (ALC M3 $<$ ALC M0) and pHL group displayed a prolonged hyperlymphocytosis (ALC M3 $>$ ALC M0) (Fig 1B). This 3-month cut-off was chosen in agreement with the RESONATE and RESONATE-2 trials, where median time to recovery from pHL was 14 and 12 weeks, respectively. Out of 122 patients treated by ibrutinib 68% were in tHL group versus 32% in pHL group in cohort 1 ($n = 41$) and 57% in tHL group versus 43% in pHL group in cohort 2 ($n = 81$) (Chi^2: 0.144) (Fig 1C). Factors significantly associated with pHL were: lower median pre-treatment ALC, absence of deletion 17p, presence of deletion 11q, and older median age but not immunoglobulin heavy chain variable region genes mutational status (S1 Fig).

Differential lymphocytosis in our series was not associated with progression-free survival (PFS) or overall survival (OS). So, we investigated patients' disposition along time of treatment exposition by swimmer plot analyses (S2 Fig). Furthermore, before 1 year of treatment, aggressive disease (Richter syndromes) occurred more frequently in tHL group (9%) than in pHL group (0%), whereas percent of CLL progression was not clearly different in both groups (6%

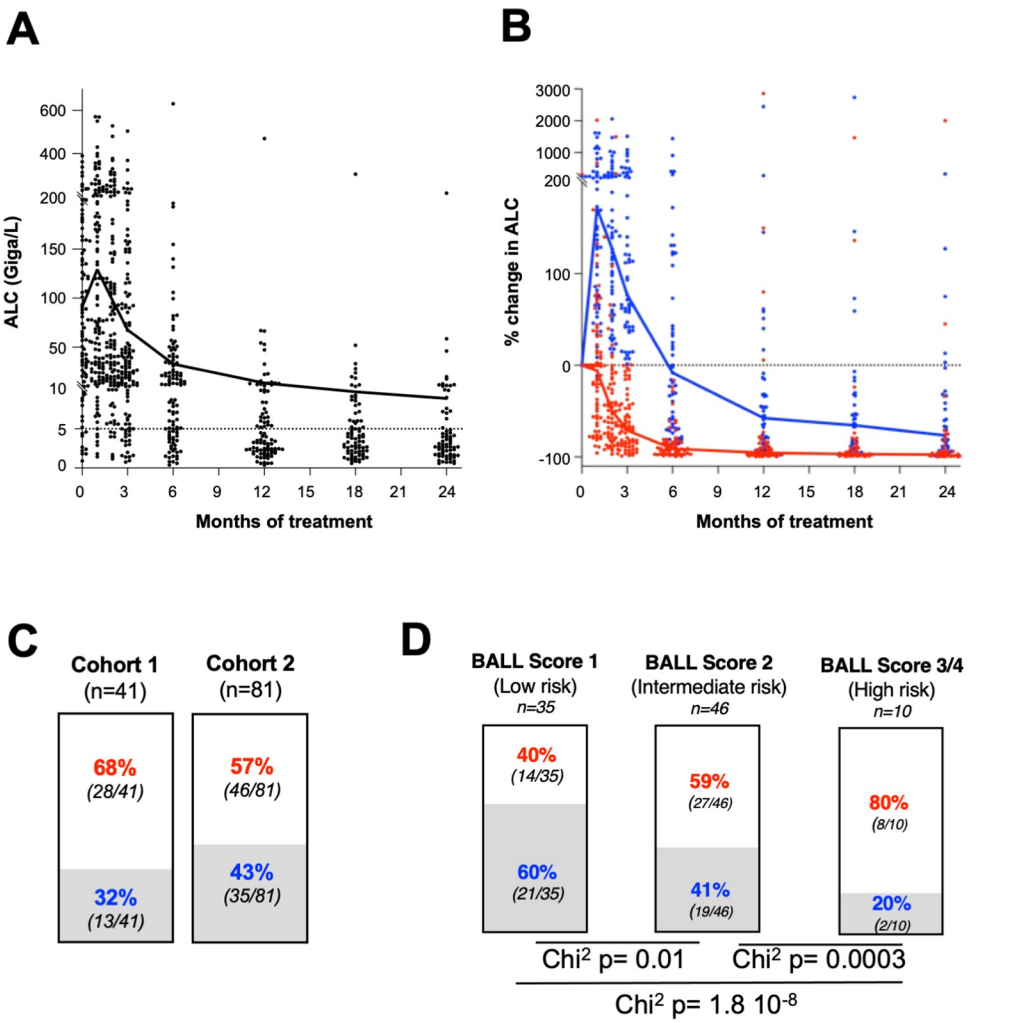

Fig 1. Ibrutinib-induced lymphocytosis. **(A)** ALC in cohort 1 (dotted line represents CLL ALC at diagnosis; black dots represent each patient at different time point; solid black lie: median). **(B)** Median of percent change in ALC compared to baseline in tHL (red line) and pHL (blue line) groups; red dots (tHL group) and blue dots (pHL group) represent each patient at different time point. **(C)** Percentage of tHL (red) and pHL (blue) groups in the 2 independent cohorts. **(D)** Percentage of tHL (red) and pHL groups (blue) according to the BALL score: low risk according to the BALL score equals a better overall survival prognosis based on 4 markers (ß2-microglobulin, Anemia, Lactacte Deshydrogenase, Last therapy) in the setting of relapsed/refractory receiving chemo-immunotherapy or targeted therapy [33]. ALC, absolute lymphocyte count; CLL, chronic lymphocytic leukemia; pHL, prolonged hyperlymphocytosis; tHL, transient hyperlymphocytosis.

https://doi.org/10.1371/journal.pmed.1004430.g001

in tHL group versus 4% in pHL group) (S4 Table). Grade 5 (lethal) adverse events occurred also more frequently in tHL group before 1 year of treatment (7% versus 0%, respectively). In addition, before 6 months, infections (Grade $\geq$ 3) were more frequent in tHL group (37%) than in pHL group (24%) ($p = 0.04$) and in relapsed/refractory patients than first-line (34% versus 15%, respectively; $p = 0.003$) (S4 Table). No correlation was found between infections and levels of B leukemic cells, $CD4^+$ and $CD8^+$ T lymphocytes, NK cells and monocytes or other clinico-biological parameters.

Interestingly, we could calculate in 91 patients (tHL group $n = 49$, pHL group $n = 42$) the BALL score [33], that is related to 4 associated factors (1 point each): ß2-microglobulin (>5 mg/L), Anemia (Hemoglobin <110 g/L), Lactacte Deshydrogenase (LDH > upper limit of

normal), Last therapy (time from initiation of last therapy < 24 months). This score has been described to predict OS under ibrutinib (irrespectively of del(11q)/del(17p) status) in relapsed/refractory CLL registration trials [34]. In our post hoc analysis, we observed that distribution of low (40% versus 60%), intermediate (59% versus 41%), and high risk (80% versus 20%) scores was statistically different between the groups (Fig 1D). Our data show that patients with pHL were overrepresented in the BALL low-risk group (60% versus 40%) and underrepresented in the high-risk group (20% versus 80%) compared with patients with tHL, suggesting that pHL group might have a better prognosis at the population level.

Baseline immune contexture and PD1 levels relate to pHL group

Monitoring of normal immune cells subsets was done in the blood of patients from cohort 1 and revealed significant differences in some cellular populations according to the groups. We could further show that baseline absolute $CD4^+$ T lymphocytes and regulatory CD4 T (Tregs) cell counts were associated with pHL (Fig 2A), but Tregs cell counts were not correlated with $CD4^+$ T lymphocytes absolute number (tHL group $R^2 = 0.009$; pHL group $R^2 = 0.05$). Furthermore, baseline PD1 level, at the surface of B leukemic lymphocytes and NK cells, was also associated with pHL (Fig 2B and 2C). As already reported [6], baseline $CD19^+/CD5^+$ level was correlated with pHL (Fig 2C). pHL group exhibited less baseline activated B leukemic cells ($CD69^+$) (Fig 2C), with respect to B leukemic cells level (tHL group $R^2 = 0.591$, $p < 0.0001$; pHL group $R^2 = 0.591$, $p = 0.003$). Finally, pHL group displayed also lower circulating B leukemic cells exhibiting lymph node features ($CD19^+/CD5^{high}/CXCR4^{low}$) (Fig 2C) that were not correlated with $CD19^+/CD5^+$ cell count (tHL group $R^2 = 0.17$, $p = 0.09$; pHL group $R^2 = 0.17$, $p = 0.44$). Baseline percentage of $PD1^+$ CLL cells before treatment was also associated to risk of infection. Indeed, infections occurred more frequently in patients with $PD1^+$ CLL cells < 20% (80% versus 42%, respectively; $p < 0.0001$).

In order to "explore" the lymph node compartment, MRI parameters were assessed in cohort 1 patients who accepted to participate to this exploration ($n = 26$). LN volumes did not significantly discriminate tHL and pHL groups (S3 Fig). Similarly, spleen volumes were not significantly different between both groups ($p = 0.928$). We also measured the ADC on the first 9 patients, before ibrutinib treatment. We observed that tHL group patients presented a higher ADC (related to lower cellularity) than patients from pHL group ($p = 0.03$) without correlation with ALC ($R^2 = 0.0005$) (S3 Fig).

Cell population dynamics during ibrutinib treatment

Evolution of cellular populations in blood was followed during ibrutinib treatment in cohort 1 (Fig 3A). Considering all patients, ibrutinib induced a decrease of all cellular populations along time of treatment. To note, T lymphocyte counts never went back to levels observed in healthy donors, even after long-term ibrutinib treatment reflecting the effect of interleukin-2-inducible T-cell kinase (ITK) targeting. In addition, even if NK cell counts decreased upon ibrutinib treatment, they remained elevated as compared to healthy donors (Fig 3A).

As observed for ALCs, ibrutinib treatment induced 2 profiles of response for all cellular populations according to tHL or pHL groups (Fig 3B). Indeed, all subsets increased rapidly in pHL group, probably due to cellular egress from lymph nodes. However, kinetic of cellular decrease was different between B and T lymphocyte populations showing that the hyperlymphocytosis of T cells in pHL group was more limited in intensity and duration than what is observed for B leukemic cells and NK subsets.

We built a mathematical model of B and T cell dynamics from cohort 1 clinical measurements. The model has been developed in several steps, by incorporating biological and medical

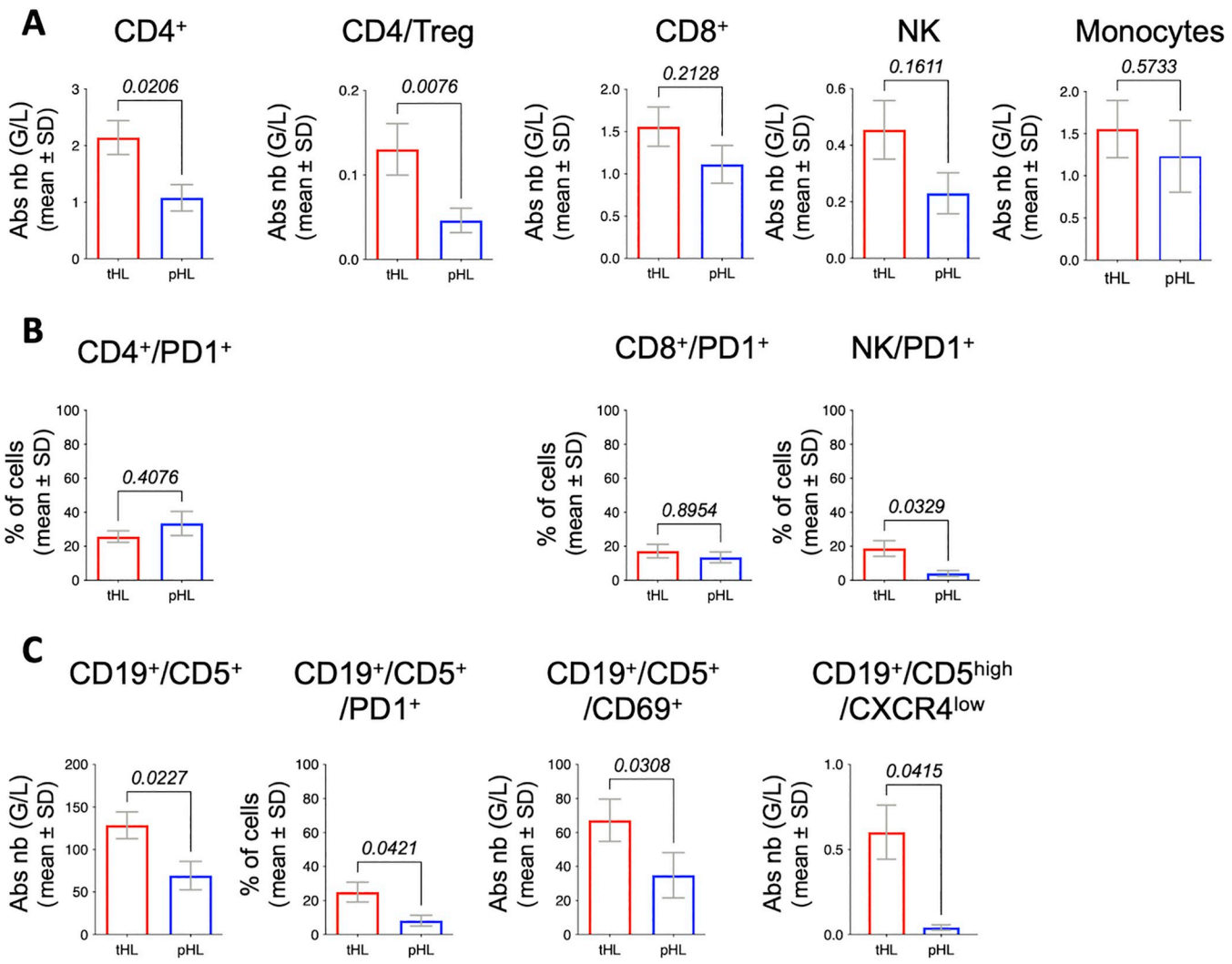

Fig 2. Immuno-phenotyping of CLL populations before ibrutinib treatment according to tHL and pHL groups. (A) Absolute number of CD4 lymphocytes, regulatory CD4 T cells (CD4/Treg), CD8 lymphocytes, Natural Killer cells (NK), and monocytes; G/L: Giga per Liter. (B) Percentage of immune cells expressing PD1. (C) Immuno-phenotyping of B leukemic cells. Abs nb, Absolute number; G/L, Giga per Liter; SD, standard deviation. For all graphs: two-tailed Mann–Whitney test between tHL group (red) and pHL group (blue). CLL, chronic lymphocytic leukemia; pHL, prolonged hyperlymphocytosis; tHL, transient hyperlymphocytosis.

https://doi.org/10.1371/journal.pmed.1004430.g002

knowledge on CLL and its treatment based on ibrutinib. Important, and sometimes prolonged, increase of B or T cell counts in blood following the onset of the treatment is observed in the cohort. Ibrutinib is known to deplete lymph nodes of leukemic B cells, so we hypothesized that not only B but also T cells exit the lymph nodes following ibrutinib treatment. Thanks to available information, we assumed that for each T cell population the flux of cells from the lymph nodes is proportional to the number of leukemic B cells in the lymph nodes (B_{LN}). This led to equations describing B and T cell dynamics, where all cell counts are normalized by their initial value (Fig 4A). A schematic representation of the model is presented in Fig 4B.

The average behavior of patients from each group is correctly reproduced (Fig 4C). Even though in both cases leukemic B cell counts in blood are overestimated from M6 after the onset of the treatment, specific dynamics of both groups are well described. The pHL characterizing pHL group is clearly visible, and is associated with high T cell counts up to M1/M2.

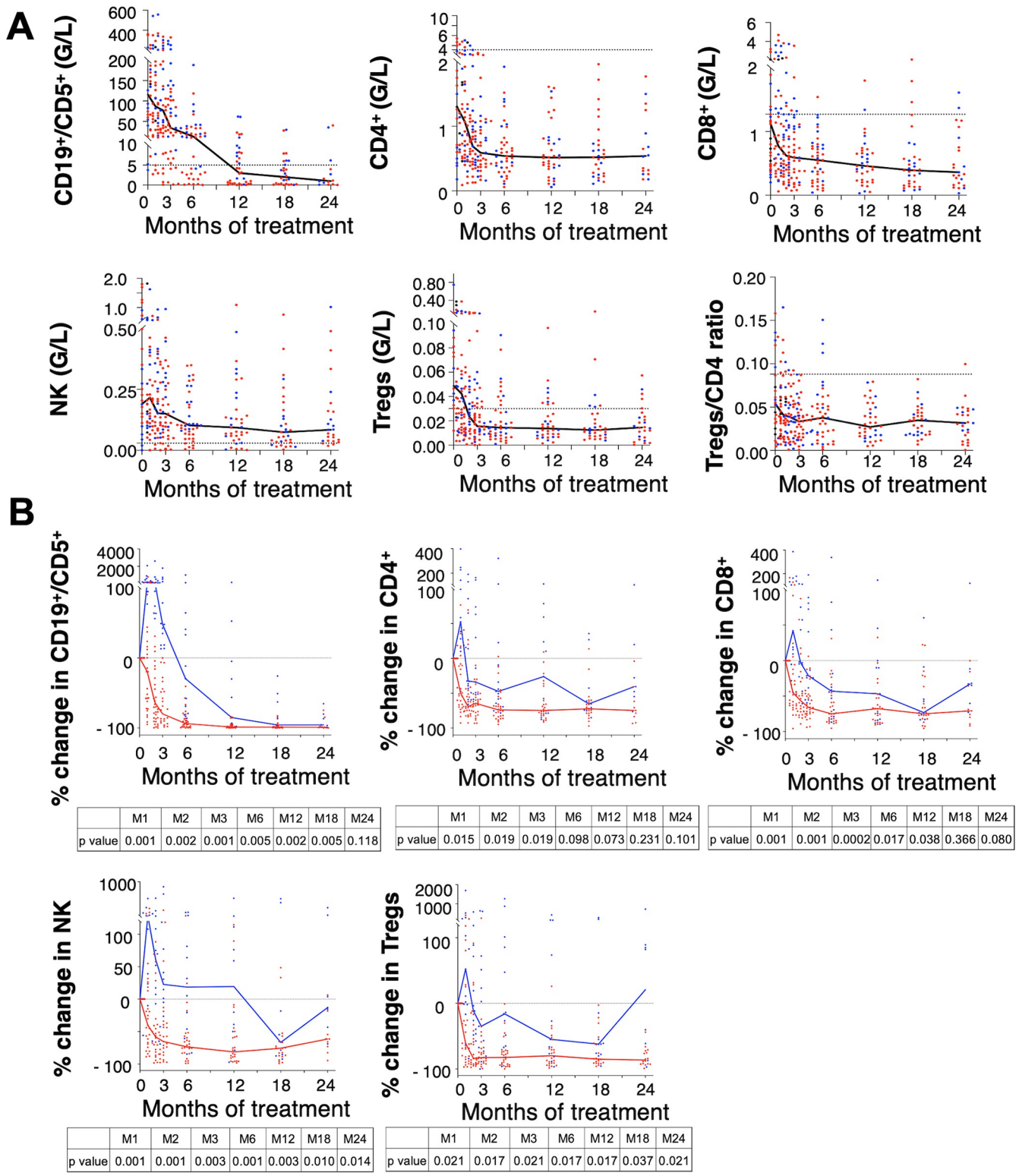

	M1	M2	M3	M6	M12	M18	M24
p value	0.001	0.002	0.001	0.005	0.002	0.005	0.118

	M1	M2	M3	M6	M12	M18	M24
p value	0.015	0.019	0.019	0.098	0.073	0.231	0.101

	M1	M2	M3	M6	M12	M18	M24
p value	0.001	0.001	0.0002	0.017	0.038	0.366	0.080

	M1	M2	M3	M6	M12	M18	M24
p value	0.001	0.001	0.003	0.001	0.003	0.010	0.014

	M1	M2	M3	M6	M12	M18	M24
p value	0.021	0.017	0.021	0.017	0.017	0.037	0.021

Fig 3. Immuno-monitoring of CLL cell populations during ibrutinib treatment. (A) Median (black line) of absolute number in leukemic B cells ($CD19^+/CD5^+$), CD4 lymphocytes, CD8 lymphocytes, Natural Killer (NK) cells, regulatory CD4 T cells (Tregs), and Tregs/CD4 ratio. In each subgraph, dotted line represents the median of absolute number of cells in healthy donors (for T lymphocytes and NK cells) and in CLL at diagnosis (B $CD19^+/CD5^+$); G/L: Giga per Liter. Red dots (tHL group) and blue dots (pHL group) represent each patient at different time point. **(B)** Median of percent change in leukemic B cells ($CD19^+/CD5^+$), CD4 lymphocytes, CD8 lymphocytes, Natural Killer (NK) cells, regulatory CD4 T cells (Tregs) compared to baseline in tHL group (red) and

pHL group (blue). G/L: Giga per Liter. Red dots (tHL group) and blue dots (pHL group) represent each patient at different time point. M1 to M24 indicate month 1 up to month 24 of treatment. Statistics: two-tailed Mann–Whitney test between tHL and pHL groups. CLL, chronic lymphocytic leukemia; pHL, prolonged hyperlymphocytosis; tHL, transient hyperlymphocytosis.

https://doi.org/10.1371/journal.pmed.1004430.g003

Dynamics of tHL group show a very brief hyperlymphocytosis (less than 1 month), associated with an increase of T cell counts on the same period. This result cannot be compared to clinical measurement yet due to lack of measurements between M0 and M1.

Parameter values estimated to fit patient's data and generate cell dynamics in Fig 4C are listed in S5 Table. The estimated values show first that T cell renewal rates are similar in both

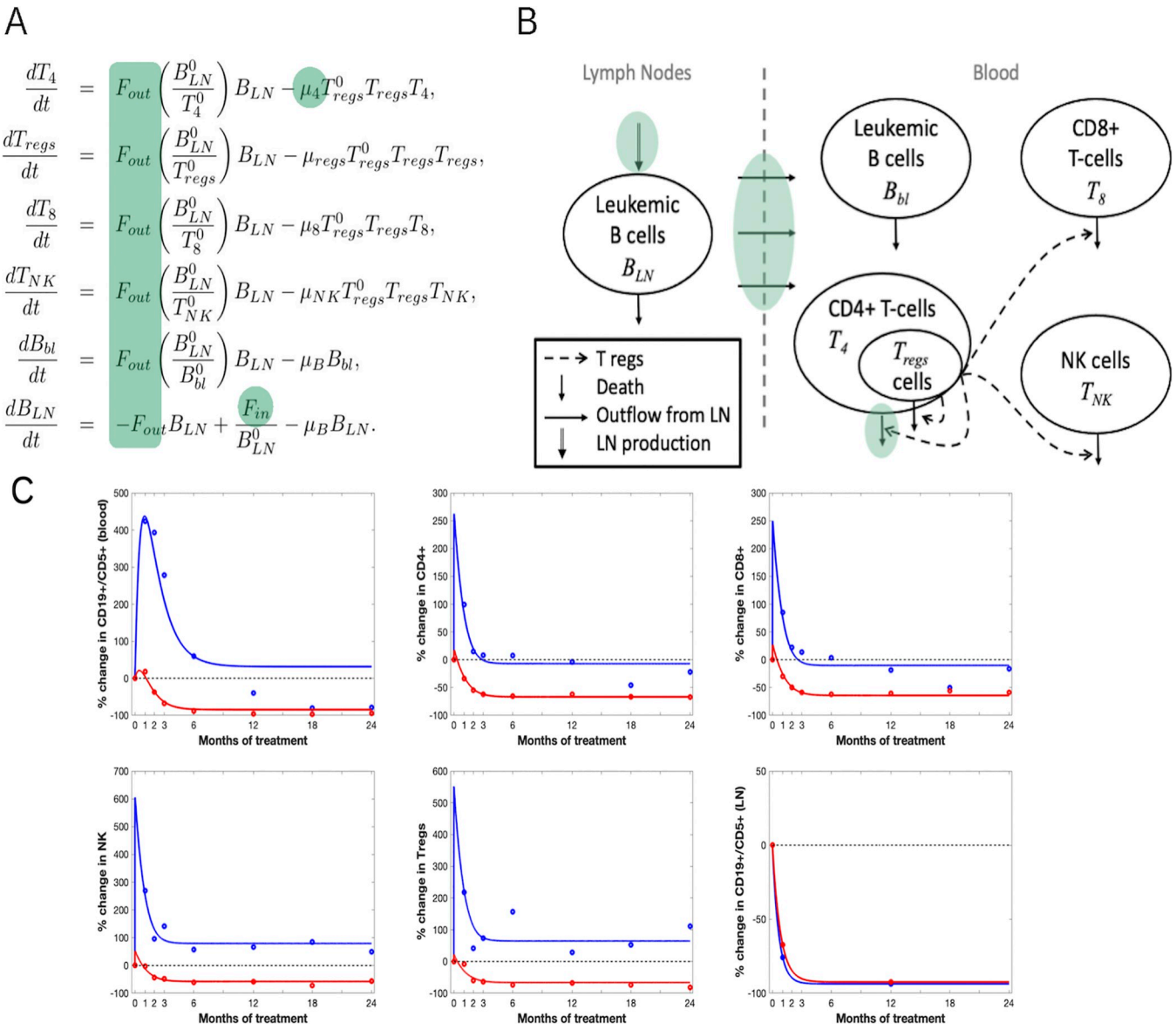

Fig 4. Mathematical model to simulate cell dynamics in CLL under ibrutinib treatment. (A) Mathematical system describing B and T cell dynamics. All variables are introduced in Table 1 and details provided in S1 File Modeling. **(B)** Schematic representation of the mathematical model. In (A) and (B), the green areas highlight the processes that depend on the groups when using the nonlinear mixed-effects model. **(C)** Both simulated (plain lines) and clinical (dots, mean values) data of B and T cell dynamics in blood are displayed, as well as B cell dynamics in lymph nodes (bottom right) in tHL group (red) and pHL group (blue). Simulated dynamics have been obtained with parameter values in S5 Table. CLL, chronic lymphocytic leukemia; LN, lymph nodes; NK, Natural Killer cells; pHL, prolonged hyperlymphocytosis; tHL, transient hyperlymphocytosis; Tregs, regulatory CD4 T cells.

https://doi.org/10.1371/journal.pmed.1004430.g004

groups, suggesting no group-specific influence of ibrutinib on T cell renewal. Second, they highlight that the main difference between both groups is in the exit rate of leukemic B cells from lymph nodes: it is 8 times larger in pHL group. Also, patients from pHL group have lower B cell death and production rates than patients from tHL group.

Based on the mathematical model built for describing average clinical measurements, we can assess that T cell count dynamics in blood are impacted by lymph node cell counts dynamics. In addition, in blood, no interaction between leukemic B cells and T cells was required to explain the observed dynamics, suggesting that these interactions can be neglected.

Biological parameters under ibrutinib treatment

In addition to a better egress of lymphoid cells in patients from pHL group, it could be also possible that B leukemic cells from these patients are less sensitive to ibrutinib due to a differential expression of BTK or its phosphorylated form. Before treatment, no difference was observed in BTK expression and pBTK/BTK ratio between both groups. In both groups, 1-month ibrutinib exposure led to a decrease of BTK protein level associated with an increase of its phosphorylated form, followed by a decrease of pBTK/BTK ratio after M6 (S4 Fig). Before treatment, in vitro depletion assays confirmed that ibrutinib induced less cell death in pHL group than in tHL group, irrespective of ibrutinib concentration (Fig 5A). In addition, ibrutinib is more efficient to $CD69^{+}$ leukemic cells in both groups (Fig 5B). Accordingly, monitoring of $CD69^{+}$ and $CD69^{-}$ showed a significantly sustained level of $CD69^{-}$ B leukemic cells in pHL group along ibrutinib exposure (Fig 5C). In addition, pHL was associated with a higher egress of B leukemic cells from lymph nodes to blood as observed by the rate of $CD5^{high}CXCR4^{low}$ circulating cells (Fig 5D), with a significant increase of $CD5^{high}CXCR4^{low}CD69^{-}$ during the first 6 months of treatment (M1 $p = 0.0003$; M2 $p < 0.0001$; M3 $p < 0.0001$; M6 $p = 0.0008$). After 2 years, all patients remaining under ibrutinib treatment decreased their lymphocytosis compared to baseline level despite some patients (27%) exhibited an ALC > 5 G/L (Fig 1A).

Mathematical modeling highlights 3 biological processes specific to pHL group

Our cohort resulted in patient-specific data for cohort 1 patients, consisting in cell counts for various cell types (B and T cells in blood and estimated B cell counts in lymph nodes) at different times after the onset of the treatment. Such data exhibit important inter-patient variability (Fig 1A). To account for it, we introduced a population approach with NLME modeling [26,30]. Contrary to the model on average data, here each patient dynamics is taken into account.

We found that the NLME model that best reproduces the measurements requires patient-specific parameters for all B and T cell processes and includes the group covariate. All T cell mortality parameters are correlated (μ_4, μ_8, μ_{NK}, μ_{reg}), as well as production and outflow of the leukemic B cells in lymph nodes (F_{in}, F_{out}). S6 Table summarizes estimated parameters.

Noticeably, F_{in}, F_{out} and μ_4 are group specific (Fig 4B), highlighting that patients from tHL and pHL groups differ significantly in their leukemic B cell dynamics within lymph nodes. Patients from pHL group are characterized by a much higher efflux rate from lymph nodes (44 times higher than in tHL group). The lymph node production rate is 5 times lower in pHL group than tHL group. Finally, $CD4^{+}$ T cell mortality rates also differ between groups, yet differences are less important (death rate 1.3 times higher in pHL group). The absence of correlation between parameters governing B and T cell dynamics shows that these dynamics are independent in blood. In addition, the death rate of leukemic B cells is the same in both groups showing that differences between both groups do not rely on this process.

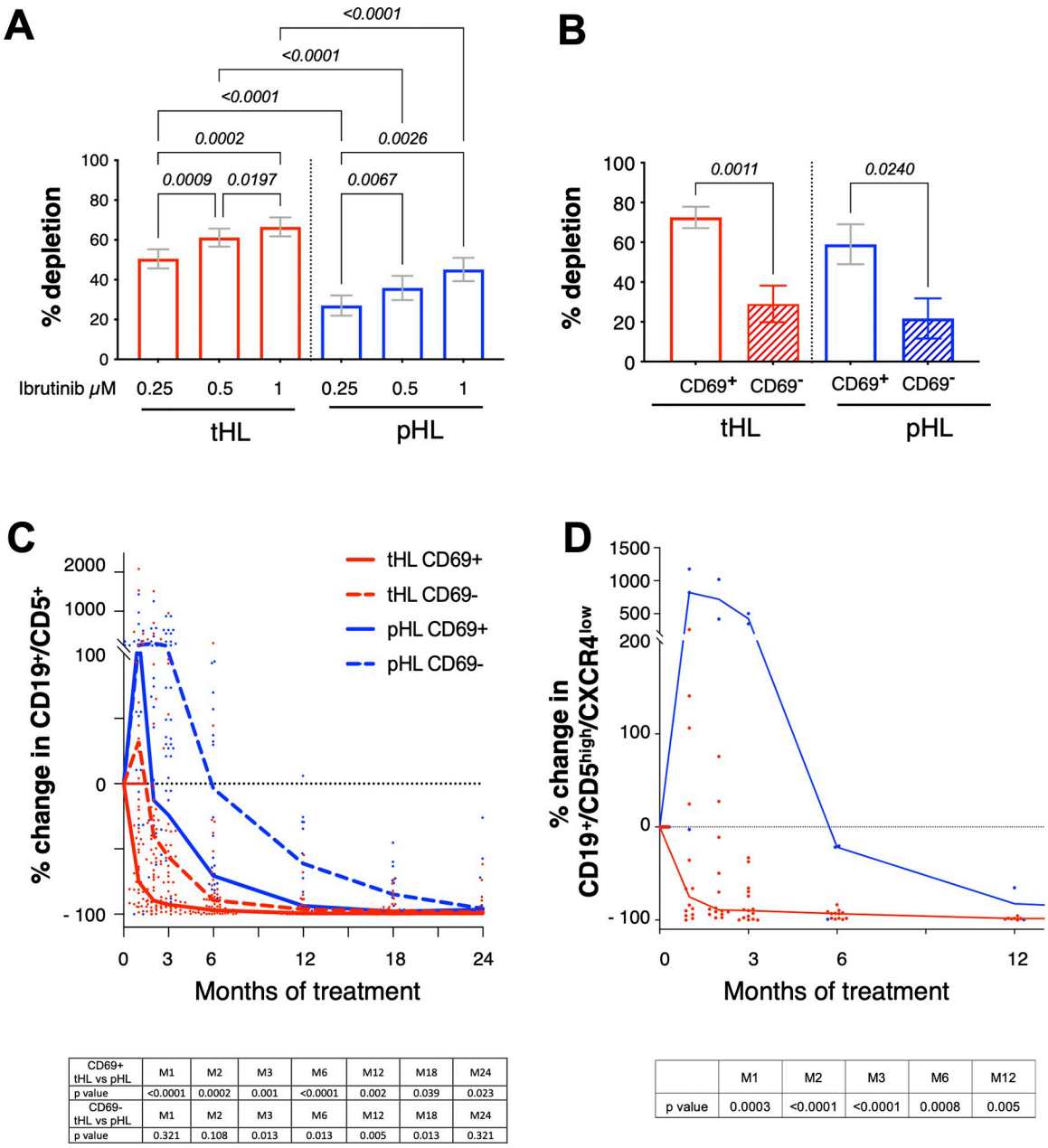

CD69+ tHL vs pHL	M1	M2	M3	M6	M12	M18	M24
p value	<0.0001	0.0002	0.001	<0.0001	0.002	0.039	0.023
CD69- tHL vs pHL	M1	M2	M3	M6	M12	M18	M24
p value	0.321	0.108	0.013	0.013	0.005	0.013	0.321

	M1	M2	M3	M6	M12
p value	0.0003	<0.0001	<0.0001	0.0008	0.005

Fig 5. In vitro ibrutinib sensitivity and egress of B leukemic cells. **(A)** In vitro dose-effect of ibrutinib on B leukemic cell depletion at M0. Statistics: two-tailed Mann–Whitney test; SD, standard deviation. **(B)** In vitro ibrutinib-sensitivity of B leukemic cells according to CD69 expression at M0. Statistics: two-tailed paired Student *t* test; SD, standard deviation. **(C)** Median (tHL group, red; pHL group, blue) of percent change of B leukemic cells, according to CD69 expression, under ibrutinib exposure. Red dots (tHL group) and blue dots (pHL group) represent each patient at different time points. Statistics: two-tailed Mann–Whitney test between tHL and pHL groups. **(D)** Median (tHL group, red; pHL group, blue) of percent change of lymph node circulating B leukemic cells during ibrutinib treatment. Red dots (tHL group) and blue dots (pHL group) represent each patient at different time points. Statistics: two-tailed Mann–Whitney test between tHL and pHL groups. pHL, prolonged hyperlymphocytosis; tHL, transient hyperlymphocytosis.

https://doi.org/10.1371/journal.pmed.1004430.g005

Fig 6 displays measured leukemic B cell counts in blood and lymph nodes for patients from tHL and pHL groups and the average cell count computed from the model. Also, individual dynamics predicted by the model were used to compute the median, the 90th and 10th percentiles. An example, for each group, of individual leukemic B cell counts in blood is displayed. It

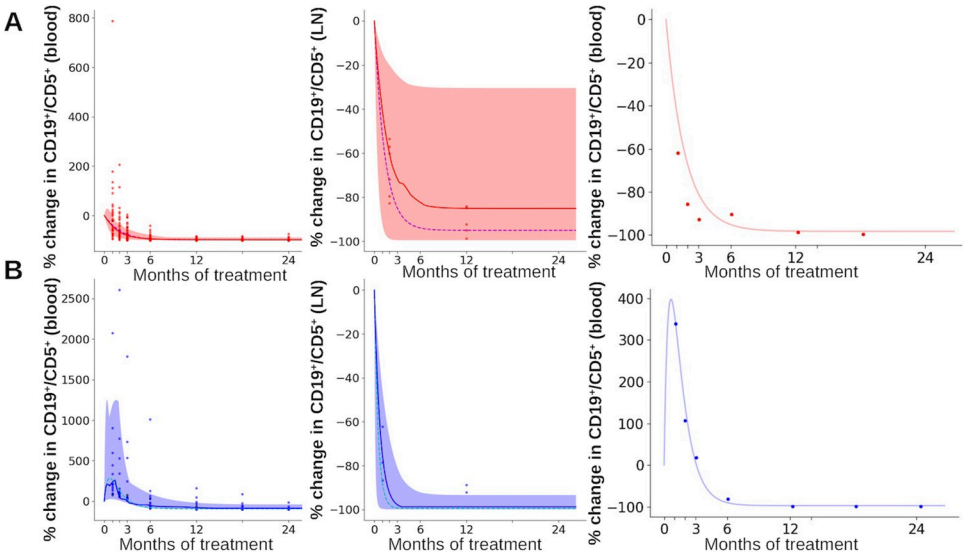

Fig 6. Model predictions of B leukemic cell evolution accounting for inter-patient variability. (A) Percent change in $CD19^+/CD5^+$ cell counts, in blood (left) and LNs (center), and an example of an individual specific dynamic displayed for $CD19^+/CD5^+$ cell counts in blood (right) in tHL group. **(B)** Percent change in $CD19^+/CD5^+$ cell counts, in blood (left) and LNs (center), and an example of an individual specific dynamic displayed for $CD19^+/CD5^+$ cell counts in blood (right) in pHL group. Dynamics are obtained from simulations of the nonlinear mixed-effects model (Fig 4A and 4B), using parameter values from S6 Table. In each plot, individual clinical measurements appear as dots. Median and mean cell counts (left, center) are represented by a straight and dashed line respectively, 10th and 90th percentiles by the colored shaded area, computed from model predictions. LN, lymph node; pHL, prolonged hyperlymphocytosis; tHL, transient hyperlymphocytosis.

https://doi.org/10.1371/journal.pmed.1004430.g006

shows the ability of the NLME model to reproduce patient-specific dynamics. It highlights the good quality of model prediction when patient variability is accounted for. Results in lymph nodes, for both groups, are impacted by the limited number of measurements. Quality of model predictions is similar for both groups.

Discussion

Our report illustrates that interdisciplinarity between biology, medical imaging, and mathematics is a strength to better understand and explain clinical observations. Indeed, in our longitudinal study and in accordance to previous clinical observations [8,9], we confirmed that ibrutinib treatment in CLL patients induced 2 patterns of response: a transient and a prolonged lymphocytosis. We highlighted the importance of tumor microenvironment in the 2 types of response and the disease course upon ibrutinib treatment for the 2 patterns of response. Indeed, we identified clinical baseline parameters (age and absolute lymphocyte counts), biological features such as absolute counts of normal immune cells ($CD4^+$ T lymphocytes, Treg cells), $CD19/CD5^{high}/CXCR4^{low}$ B leukemic cells, PD1 and CD69 expression on B leukemic hyperlymphocytosis and lymph node cellularity assessing by whole body MRI. We also pinpointed that the group of patients identified by the transient hyperlymphocytosis had lower duration response and a poor clinical outcome. By developing the mathematical model, we confirmed the role of the balance between cell death and cell egress from lymph nodes in the response to ibrutinib treatment. Noticeably, this study was not based on statistical dichotomization of patients but built on previous clinical reports, defining the 2 groups of response under ibrutinib treatment. Nevertheless, the model confirmed cell counts evolution of B leukemic cells [5,7] and provided new information on T lymphocytes dynamics in CLL patients

upon ibrutinib treatment. Thus, our study gave a better knowledge of ibrutinib response in CLL patients and provided information for clinicians to better manage ibrutinib therapy, especially in the first 3 months of treatment.

Our study relied on ALCs-based groups of response to treatment, with groups either exhibiting pHL (ALC M3 > ALC M0) or tHL (ALC M3 < ALC M0). Similar definition of groups of patients was previously introduced in clinical studies [6,8–10]. In this work as well as in previous ones [6,8–10], dichotomization of patients in 2 groups has not been performed based on a statistical criterion. Indeed, statistical methods could be used to determine whether 2 or more groups of patients can be extracted from the data, and if so, what would be the optimal criterion to define the groups. For instance, mixture models with different numbers of components could be fit to the data [35,36]. Since distributions of ALCs are highly skewed to the right (few patients with very high ALCs), it is however important to account for this specific feature of the data that make them unlikely to be fitted by Gaussian distributions. We nevertheless decided to use group definitions introduced in the literature, since they represented clinical practice and consequently had potential easy clinical applications by helping to better stratify and follow patients during ibrutinib treatment. In addition, it may be noted that ALC data were not normally distributed (Shapiro–Wilk test, not shown) and did not have the same laws (Wilcoxon Mann–Whitney test, not shown) at M0, M2, and M3, suggesting that the 2 groups identified different treatment responses.

Since this study was based on only 1 measurement per time point and per patient, it was therefore not possible to estimate the regression to the mean effect [37] in measured ALCs and groups definition. However, over the 122 patients of both cohorts 1 and 2, dynamics over the 3 first months after treatment (measurements M1, M2, and M3) remained the same for 90 patients (that is, either above or below baseline). We could then assume that the variations on which groups of responses had been constructed were mostly due to the treatment effect and could not be explained by regression to the mean effect only.

Introducing a mathematical model to describe cell counts evolution in CLL patients treated with ibrutinib was an original and complementary approach to the current clinical study. We chose to introduce an NLME model to characterize each patient profile instead of independently fitting our model to individual patient data. Indeed, such an approach would have been limited by missing data that could prevent model parameters identifiability. The NLME approach used efficiently the available information from existing measurements. Estimated values for leukemic B cell death rate and the exit rate from lymph nodes were of the same order of magnitude than the ones reported in Wodarz and colleagues [5] and Burger and colleagues [7]. We additionally described T lymphocytes dynamics under ibrutinib hence characterizing more specifically the effect of ibrutinib treatment on CLL patients. We found that T cell mortality parameters are correlated, with higher correlation rates for $CD4^+$/$CD8^+$ T cells and regulatory CD4 T cells. To confirm its robustness, the model should be compared to a new and larger dataset.

By targeting ITK, ibrutinib also induced 2 groups of response in normal cells. This suggested that ibrutinib sensitivity and/or activation/exhaustion status of normal cells may affect the dynamic of efflux versus production rates as well as cell death. Indeed, the observed baseline of absolute $CD4^+$ T cell counts was significantly smaller in pHL group. It was estimated, with the mathematical model, that the death rate of $CD4^+$ T cells was higher in pHL group, contributing to explain the differences observed between groups. For each group, neither basal nor time-course level of immune cells were correlated to ALCs and, except for Natural Killer cells, absolute number of immune cells was always lower than in healthy donors. Even though T lymphocytes function was under the scope of our study, results from clinical trials using CD19/CD3 bispecific antibody [38] showed that immune cells were efficient against ibrutinib-

resistant B leukemic cells. This suggested that despite a drastic reduction of T lymphocytes number by ibrutinib treatment, function was not completely altered. It would be interesting to follow immune cells time-course under new BTK inhibitors (acalabrutinib [39], zanubrutinib [40]), which induced a lesser inhibition of ITK.

In order to explain the differential response to ibrutinib, we addressed the hypothesis that lymph node micro-environment composition and related-cellularity, measured by the ADC, could be different between groups. Our results showed that patients from tHL group present a higher ADC (related to lower cellularity) than patients from pHL group without correlation with ALCs. These preliminary data should be validated in a larger cohort of patients to characterize ADC as a predictive marker of ibrutinib response evolution and its use in clinical practice. However, we can speculate that in tHL group, the structure of lymph nodes may be less compact, promoting, at least in part, the exit of cells into blood compartment before treatment. Conversely, a lower ADC (related to higher cellularity) in pHL group could be linked to a more compact structure of lymph nodes in these patients and so, a basal lower egress of cells into blood. This hypothesis is reinforced by absolute lymphocyte quantification and the high number of circulating CD19/CD5^{high}/CXCR4^{low} cells in tHL group versus pHL group before treatment. Then, during ibrutinib treatment, a lower compaction of lymph nodes could promote a better diffusion of ibrutinib into these organs, leading to an increase of cell death in situ, and a reduced egress of leukemic cells (as observed in tHL group). On the contrary, a higher compaction of lymph nodes (pHL group) could decrease ibrutinib diffusion and efficiency, leading to a more prolonged egress of cells from lymph nodes to the blood compartment. However, this phenomenon could also be coupled to chemokine sensitivity and surface proteins, such as CD69, S1P1, CCR7 [41–45] that contribute to cellular egress or retention in CLL lymph nodes. Finally, the pHL during treatment could also be linked to the lesser sensitivity of CD69^{-} B leukemic cells to ibrutinib.

Mathematical results supported the biological parameters associated with pHL and the previous hypotheses. Under ibrutinib treatment, the lymph node exit rate of leukemic B cells was much higher in pHL group than in tHL group. In addition, the observed smaller leukemic B cell number in pHL group (less baseline activated leukemic B cells CD69^{+} and circulating leukemic B cells with lymph node features (CD19^{+}/CD5^{high}/CXCR4^{low})) could be explained by a smaller production rate in lymph nodes that was mathematically estimated to a lower value in pHL group than in tHL group. The mathematical analysis also highlighted that inter-patient variability was not sufficient to explain the differences between the 2 groups. This means that differences observed in measurements were mainly due to a significant difference in the biological processes between the 2 groups of patients.

Our study also pinpointed that blood lymphocytosis induced by ibrutinib is associated to duration response and outcomes. Indeed, pHL identified a group with a better prognosis (Fig 1) [8,10]. This observation could be related to the concept of inter-clonal equilibrium/competition among B leukemic clones leading to the non-expansion of a dominant clone (BTK mutated or more proliferating) [46–48].

Altogether, our study provides a better understanding of which baseline clinico-biological and pharmaco-dynamic parameters dictate absolute lymphocyte kinetics upon ibrutinib treatment. Combining MRI and standard procedures (such as minimal residual disease in blood and bone marrow compartments) might help to design future clinical trials with a more thorough evaluation of "tissular compartments" responses. As our results highlight suboptimal outcomes in patients with transient hyperlymphocytosis, we believe that our approach could provide a support for choosing whether ibrutinib should be given alone or associated with, for instance, venetoclax (this combo is approved by EMEA, not yet FDA) or other therapies after 3 months.

Supporting information

S1 STROBE Checklist. STROBE Statement—checklist of items that should be included in reports of observational studies.
(PDF)

S1 Table. Antibodies used in the study.
(PDF)

S2 Table. Initial configurations of nonlinear mixed-effects (nlme) models used with SAMBA. The second column indicates which error model has been used (Constant or Proportional). The third column indicates which random effects (r.e) were accounted for. The fourth column indicates which correlations were considered. The fifth column indicates whether covariates were included, and if so on which parameters. Parameters are described in Table 1 (main text).
(PDF)

S3 Table. Clinical characteristics of patients. tHL, transient hyperlymphocytosis group; pHL, prolonged hyperlymphocytosis group. Nb, number; Tt, treatment; LN, lymph nodes.
(PDF)

S4 Table. Clinical outcome of CLL patients according to transient hyperlymphocytosis (tHL) and prolonged hyperlymphocytosis (pHL) groups. Nb, number.
(PDF)

S5 Table. Parameter values associated with the best fit of average clinical data for both transient hyperlymphocytosis (tHL) and prolonged hyperlymphocytosis (pHL) groups and used in Fig 4C. Parameters are described in Table 1 (main text). (CI—confidence intervals, based on the profile likelihood; d–day).
(PDF)

S6 Table. Parameter values associated with the best fit of individual patient measurements. Values are averaged over 10 runs with different initial guess. Parameters are described in Table 1 (main text) and in S1 File Modeling. For fixed parameters F_{out}, F_{in} and μ_4, superscripts t and p refer to tHL (transient hyperlymphocytosis) and pHL (prolonged hyperlymphocytosis) groups, respectively, identified by a covariate (see Section 2.2 in S1 File Modeling). Coefficient $c(x, y)$ is the correlation coefficient between x and y computed by Monolix (see section 2.1 in S1 File Modeling). (SD–standard deviation; LL–log-likelihood; d–day; NU—no unit).
(PDF)

S1 Fig. Analysis of factors associated with hyperlymphocytosis. Median of percent change in age **(A)** and absolute lymphocyte counts (ALCs) **(B)** (insert: according to cohort 1 and 2) in transient hyperlymphocytosis (tHL) and prolonged hyperlymphocytosis (pHL) groups; each dot represents a patient. **(C)** Percent of patients in tHL (red) and pHL (blue) groups according to genetic alterations. Del: deletion; IGHV M: mutated immunoglobulin heavy chain variable region genes; IGHV UM: unmutated immunoglobulin heavy chain variable region genes.
(PDF)

S2 Fig. Long-term evolution of patients under ibrutinib therapy. Transient hyperlymphocytosis group (tHL) ($n = 68$); prolonged hyperlymphocytosis group (pHL) ($n = 52$); each line represents a patient.
(PDF)

S3 Fig. Magnetic resonance imaging (MRI) analysis before ibrutinib treatment. (A) Representative features of total body MRI for a patient before ibrutinib treatment. Arbitrary colors

indicate the different organs of interest (cervical, axillary, mediastinal, retroperitoneal, iliac lymph nodes, spleen, and liver). **(B)** Volume of lymph nodes according to transient hyperlymphocytosis group (tHL) and prolonged hyperlymphocytosis group (pHL). **(C)** ADC of lymph nodes according to tHL and pHL groups. SD, standard deviation.
(PDF)

S4 Fig. Monitoring of phosphoBTK/BTK along ibrutinib treatment. tHL, transient hyperlymphocytosis group; pHL, prolonged hyperlymphocytosis group; SD, standard deviation; a. u., arbitrary units.
(PDF)

S1 File Modeling. Model construction, parameter estimation, model selection. Details on modeling choices, parameter estimation methodology, model selection procedure, for both the generic model and the patient-specific model.
(PDF)

Acknowledgments

The authors thank the patients who participated in this study, Sandra Debarros (Clinical Research Associate IUCT-O) and Sebastien Gadat (TSE, Toulouse). The authors are grateful to Dr. Melanie Prague for sharing her expertise on nonlinear mixed effect modeling and SAMBA use with R.

Author Contributions

Conceptualization: Chloe Audebert, Fabien Crauste, Anne Quillet-Mary.

Data curation: Chloe Audebert, Charlotte Dion, Soleakhena Ken, Fabien Crauste, Anne Quillet-Mary.

Formal analysis: Chloe Audebert, Charlotte Dion, Soleakhena Ken, Fabien Crauste.

Funding acquisition: Loic Dupré, Loic Ysebaert, Fabien Crauste, Anne Quillet-Mary.

Investigation: Sarah Cadot, Soleakhena Ken, Laetitia Largeaud, Anne Quillet-Mary.

Methodology: Sarah Cadot, Chloe Audebert, Charlotte Dion, Laetitia Largeaud, Fabien Crauste, Anne Quillet-Mary.

Project administration: Loic Ysebaert, Anne Quillet-Mary.

Resources: Loic Ysebaert, Anne Quillet-Mary.

Software: Chloe Audebert, Charlotte Dion, Soleakhena Ken, Fabien Crauste.

Supervision: Anne Quillet-Mary.

Validation: Sarah Cadot, Chloe Audebert, Soleakhena Ken, Fabien Crauste, Anne Quillet-Mary.

Visualization: Sarah Cadot, Chloe Audebert, Fabien Crauste, Anne Quillet-Mary.

Writing – original draft: Sarah Cadot, Chloe Audebert, Soleakhena Ken, Loic Ysebaert, Fabien Crauste, Anne Quillet-Mary.

Writing – review & editing: Sarah Cadot, Chloe Audebert, Charlotte Dion, Soleakhena Ken, Loic Dupré, Laetitia Largeaud, Camille Laurent, Loic Ysebaert, Fabien Crauste, Anne Quillet-Mary.

References

1. Burger JA, O'Brien S. Evolution of CLL treatment—from chemoimmunotherapy to targeted and individualized therapy. Nat Rev Clin Oncol. 2018 Aug; 15(8):510–527. https://doi.org/10.1038/s41571-018-0037-8 PMID: 29777163
2. Byrd JC, Furman RR, Coutre SE, Flinn IW, Burger JA, Blum K, et al. Ibrutinib Treatment for First-Line and Relapsed/Refractory Chronic Lymphocytic Leukemia: Final Analysis of the Pivotal Phase Ib/II PCYC-1102 Study. Clin Cancer Res. 2020 Aug 1; 26(15):3918–3927. https://doi.org/10.1158/1078-0432.CCR-19-2856 PMID: 32209572
3. ten Hacken E, Burger JA. Molecular Pathways: Targeting the Microenvironment in Chronic Lymphocytic Leukemia—Focus on the B-Cell Receptor. Clin Cancer Res. 2014 Feb 1; 20(3):548–556. https://doi.org/10.1158/1078-0432.CCR-13-0226 PMID: 24323900
4. Niemann CU, Herman SEM, Maric I, Gomez-Rodriguez J, Biancotto A, Chang BY, et al. Disruption of in vivo Chronic Lymphocytic Leukemia Tumor–Microenvironment Interactions by Ibrutinib–Findings from an Investigator-Initiated Phase II Study. Clin Cancer Res. 2016 Apr 1; 22(7):1572–1582. https://doi.org/10.1158/1078-0432.CCR-15-1965 PMID: 26660519
5. Wodarz D, Garg N, Komarova NL, Benjamini O, Keating MJ, Wierda WG, et al. Kinetics of CLL cells in tissues and blood during therapy with the BTK inhibitor ibrutinib. Blood. 2014 Jun 26; 123(26):4132–4135. https://doi.org/10.1182/blood-2014-02-554220 PMID: 24829205
6. Herman SEM, Niemann CU, Farooqui M, Jones J, Mustafa RZ, Lipsky A, et al. Ibrutinib-induced lymphocytosis in patients with chronic lymphocytic leukemia: correlative analyses from a phase II study. Leukemia. 2014 Nov; 28(11):2188–2196. https://doi.org/10.1038/leu.2014.122 PMID: 24699307
7. Burger JA, Li KW, Keating MJ, Sivina M, Amer AM, Garg N, et al. Leukemia cell proliferation and death in chronic lymphocytic leukemia patients on therapy with the BTK inhibitor ibrutinib. JCI Insight. 2017;2 (2).
8. Barrientos JC, Burger JA, Byrd JC, Hillmen P, Zhou C, Ninomoto J, et al. Characterizing the kinetics of lymphocytosis in patients with chronic lymphocytic leukemia treated with single-agent ibrutinib. Leuk Lymphoma. 2019 Mar 21; 60(4):1000–1005. https://doi.org/10.1080/10428194.2018.1512710 PMID: 30277101
9. Brown JR, Hillmen P, O'Brien S, Barrientos JC, Reddy NM, Coutre SE, et al. Extended follow-up and impact of high-risk prognostic factors from the phase 3 RESONATE study in patients with previously treated CLL/SLL. Leukemia. 2018 Jan; 32(1):83–91. https://doi.org/10.1038/leu.2017.175 PMID: 28592889
10. Munir T, Brown JR, O'Brien S, Barrientos JC, Barr PM, Reddy NM, et al. Final analysis from RESONATE: Up to six years of follow-up on ibrutinib in patients with previously treated chronic lymphocytic leukemia or small lymphocytic lymphoma. Am J Hematol. 2019 Dec; 94(12):1353–1363. https://doi.org/10.1002/ajh.25638 PMID: 31512258
11. Lipsky AH, Farooqui MZH, Tian X, Martyr S, Cullinane AM, Nghiem K, et al. Incidence and risk factors of bleeding-related adverse events in patients with chronic lymphocytic leukemia treated with ibrutinib. Haematologica. 2015 Dec 1; 100(12):1571–1578. https://doi.org/10.3324/haematol.2015.126672 PMID: 26430171
12. Levade M, David E, Garcia C, Laurent PA, Cadot S, Michallet AS, et al. Ibrutinib treatment affects collagen and von Willebrand factor-dependent platelet functions. Blood. 2014 Dec 18; 124(26):3991–3995. https://doi.org/10.1182/blood-2014-06-583294 PMID: 25305202
13. Riches JC, Davies JK, McClanahan F, Fatah R, Iqbal S, Agrawal S, et al. T cells from CLL patients exhibit features of T-cell exhaustion but retain capacity for cytokine production. Blood. 2013 Feb 28; 121(9):1612–1621. https://doi.org/10.1182/blood-2012-09-457531 PMID: 23247726
14. Pleyer C, Wiestner A, Sun C. Immunological changes with kinase inhibitor therapy for chronic lymphocytic leukemia. Leuk Lymphoma. 2018 Dec 2; 59(12):2792–2800. https://doi.org/10.1080/10428194.2018.1457147 PMID: 29764250
15. Long M, Beckwith K, Do P, Mundy BL, Gordon A, Lehman AM, et al. Ibrutinib treatment improves T cell number and function in CLL patients. J Clin Invest. 2017 Jul 17; 127(8):3052–3064. https://doi.org/10.1172/JCI89756 PMID: 28714866
16. Fraietta JA, Beckwith KA, Patel PR, Ruella M, Zheng Z, Barrett DM, et al. Ibrutinib enhances chimeric antigen receptor T-cell engraftment and efficacy in leukemia. Blood. 2016 Mar 3; 127(9):1117–1127. https://doi.org/10.1182/blood-2015-11-679134 PMID: 26813675
17. Parry HM, Mirajkar N, Cutmore N, Zuo J, Long H, Kwok M, et al. Long-Term Ibrutinib Therapy Reverses CD8+ T Cell Exhaustion in B Cell Chronic Lymphocytic Leukaemia. Front Immunol. 2019 Dec 12; 10:2832.

18. Kondo K, Shaim H, Thompson PA, Burger JA, Keating M, Estrov Z, et al. Ibrutinib modulates the immunosuppressive CLL microenvironment through STAT3-mediated suppression of regulatory B-cell function and inhibition of the PD-1/PD-L1 pathway. Leukemia. 2018 Apr; 32(4):960–970. https://doi.org/10.1038/leu.2017.304 PMID: 28972595

19. Komarova NL, Burger JA, Wodarz D. Evolution of ibrutinib resistance in chronic lymphocytic leukemia (CLL). Proc Natl Acad Sci U S A. 2014 Sep 23; 111(38):13906–13911. https://doi.org/10.1073/pnas.1409362111 PMID: 25201956

20. Laprevotte E, Ysebaert L, Klein C, Valleron W, Blanc A, Gross E, et al. Endogenous IL-8 acts as a CD16 co-activator for natural killer-mediated anti-CD20 B cell depletion in chronic lymphocytic leukemia. Leuk Res. 2013 Apr; 37(4):440–446. https://doi.org/10.1016/j.leukres.2012.11.015 PMID: 23259986

21. Grossiord E, Risser L, Kanoun S, Aziza R, Chiron H, Ysebaert L, et al. Semi-automatic segmentation of whole-body images in longitudinal studies. Biomed Phys Eng Express. 2021 Jan 1; 7(1):015014.

22. Raue A, Steiert B, Schelker M, Kreutz C, Maiwald T, Hass H, et al. Data2Dynamics: a modeling environment tailored to parameter estimation in dynamical systems. Bioinformatics. 2015 Nov 1; 31(21):3558–3560. https://doi.org/10.1093/bioinformatics/btv405 PMID: 26142188

23. Raue A, Schilling M, Bachmann J, Matteson A, Schelke M, Kaschek D, et al. Lessons Learned from Quantitative Dynamical Modeling in Systems Biology. Hernandez-Lemus E, editor. PLoS ONE. 2013 Sep 30; 8(9):e74335. https://doi.org/10.1371/journal.pone.0074335 PMID: 24098642

24. Raue A, Kreutz C, Maiwald T, Bachmann J, Schilling M, Klingmüller U, et al. Structural and practical identifiability analysis of partially observed dynamical models by exploiting the profile likelihood. Bioinformatics. 2009 Aug 1; 25(15):1923–1929. https://doi.org/10.1093/bioinformatics/btp358 PMID: 19505944

25. Garnett GP, Cousens S, Hallett TB, Steketee R, Walker N. Mathematical models in the evaluation of health programmes. Lancet. 2011 Aug; 378(9790):515–525. https://doi.org/10.1016/S0140-6736(10)61505-X PMID: 21481448

26. Lavielle M. Mixed effects models for the population approach. Models, Tasks, Methods and Tools. In: Chapmann and Hall/CRC. 2014.

27. Delyon B, Lavielle M, Moulines E. Convergence of a stochastic approximation version of the EM algorithm. Ann Stat. 1999; 27(1):94–128.

28. Kuhn E, Lavielle M. Maximum likelihood estimation in nonlinear mixed effects models. Comput Stat Data Anal. 49(4):1020–1038.

29. Samson A, Donnet S. Estimation of parameters in incomplete data models defined by dynamical systems. J Stat Plan Inference. 2007; 137(9):2815–2831.

30. Monolix version 2019R1Antony. France: Lixoft SAS. 2019.

31. Prague M, Lavielle M. SAMBA: A novel method for fast automatic model building in nonlinear mixed-effects models. CPT Pharmacometrics Syst Pharmacol. 2022 Feb; 11(2):161–72. https://doi.org/10.1002/psp4.12742 PMID: 35104058

32. Lavielle M. Rsmlx: R Speaks 'Monolix' [Internet]. 2021. Available from: http://rsmlx.webpopix.org. R package version 4.0.2.

33. Soumerai JD, Ni A, Darif M, Londhe A, Xing G, Mun Y, et al. Prognostic risk score for patients with relapsed or refractory chronic lymphocytic leukaemia treated with targeted therapies or chemoimmunotherapy: a retrospective, pooled cohort study with external validations. Lancet Haematol. 2019 Jul; 6(7):e366–e374. https://doi.org/10.1016/S2352-3026(19)30085-7 PMID: 31109827

34. Ysebaert L, Michallet AS, Bijou F, Clavert A, Quinquenel A, Calleja A, et al. Real-World Ibrutinib Validation of the Ball Score to Predict Overall Survival: A Filo Group Study in RR CLL Patients. Blood. 2019 Nov 13; 134(1):1741–1741.

35. McLachlan GJ, Rathnayake S. On the number of components in a Gaussian mixture model. WIREs Data Min Knowl. 2014 Sep; 4(5):341–355.

36. Scrucca L, Fraley C, Murphy TB, Adrian E. R. Model-Based Clustering, Classification, and Density Estimation Using mclust in R. 1st ed. Boca Raton: Chapman and Hall/CRC; 2023.

37. Barnett AG. Regression to the mean: what it is and how to deal with it. Int J Epidemiol. 2004 Aug 27; 34(1):215–220. https://doi.org/10.1093/ije/dyh299 PMID: 15333621

38. Robinson HR, Qi J, Cook EM, Nichols C, Dadashian EL, Underbayev C, et al. A CD19/CD3 bispecific antibody for effective immunotherapy of chronic lymphocytic leukemia in the ibrutinib era. Blood. 2018 Aug 2; 132(5):521–532. https://doi.org/10.1182/blood-2018-02-830992 PMID: 29743179

39. Byrd JC, Harrington B, O'Brien S, Jones JA, Schuh A, Devereux S, et al. Acalabrutinib (ACP-196) in Relapsed Chronic Lymphocytic Leukemia. N Engl J Med. 2016 Jan 28; 374(4):323–332. https://doi.org/10.1056/NEJMoa1509981 PMID: 26641137

40. Shadman M, Flinn IW, Levy MY, Porter RF, Burke JM, Zafar SF, et al. Zanubrutinib in patients with previously treated B-cell malignancies intolerant of previous Bruton tyrosine kinase inhibitors in the USA: a phase 2, open-label, single-arm study. Lancet Haematol. 2023 Jan; 10(1):e35–e45. https://doi.org/10.1016/S2352-3026(22)00320-9 PMID: 36400069

41. Bankovich AJ, Shiow LR, Cyster JG. CD69 Suppresses Sphingosine 1-Phosophate Receptor-1 (S1P1) Function through Interaction with Membrane Helix 4. J Biol Chem. 2010 Jul; 285(29):22328–22337. https://doi.org/10.1074/jbc.M110.123299 PMID: 20463015

42. Shiow LR, Rosen DB, Brdičková N, Xu Y, An J, Lanier LL, et al. CD69 acts downstream of interferon-α/β to inhibit S1P1 and lymphocyte egress from lymphoid organs. Nature. 2006 Mar; 440(7083):540–544.

43. Cyster JG, Schwab SR. Sphingosine-1-Phosphate and Lymphocyte Egress from Lymphoid Organs. Annu Rev Immunol. 2012 Apr 23; 30(1):69–94. https://doi.org/10.1146/annurev-immunol-020711-075011 PMID: 22149932

44. Patrussi L, Capitani N, Martini V, Pizzi M, Trimarco V, Frezzato F, et al. Enhanced Chemokine Receptor Recycling and Impaired S1P1 Expression Promote Leukemic Cell Infiltration of Lymph Nodes in Chronic Lymphocytic Leukemia. Cancer Res. 2015 Oct 1; 75(19):4153–4163. https://doi.org/10.1158/0008-5472.CAN-15-0986 PMID: 26282174

45. Rey-Barroso J, Munaretto A, Rouquié N, Mougel A, Chassan M, Gadat S, et al. Lymphocyte migration and retention properties affected by ibrutinib in chronic lymphocytic leukemia. Haematologica. 2023 Jun 29; 109(3):809–823.

46. Gutierrez C, Wu CJ. Clonal dynamics in chronic lymphocytic leukemia. Blood Adv. 2019 Nov 26; 3(22):3759–3769. https://doi.org/10.1182/bloodadvances.2019000367 PMID: 31770443

47. Condoluci A, Rossi D. Genomic Instability and Clonal Evolution in Chronic Lymphocytic Leukemia: Clinical Relevance. J Natl Compr Canc Netw. 2021 Feb; 19(2):227–233.

48. Landau DA, Sun C, Rosebrock D, Herman SEM, Fein J, Sivina M, et al. The evolutionary landscape of chronic lymphocytic leukemia treated with ibrutinib targeted therapy. Nat Commun. 2017 Dec 19; 8(1):2185. https://doi.org/10.1038/s41467-017-02329-y PMID: 29259203

STROBE Statement—checklist of items that should be included in reports of observational studies

	Item No	Recommendation	Relevant text from manuscript
Title and abstract	1	(*a*) Indicate the study's design with a commonly used term in the title or the abstract	Title; abstract, paragraph 2
		(*b*) Provide in the abstract an informative and balanced summary of what was done and what was found	Abstract, paragraphs 2-3
Introduction			
Background/rationale	2	Explain the scientific background and rationale for the investigation being reported	Introduction, paragraphs 1-4
Objectives	3	State specific objectives, including any prespecified hypotheses	Introduction, paragraph 5
Methods			
Study design	4	Present key elements of study design early in the paper	Method, paragraphs 1-4
Setting	5	Describe the setting, locations, and relevant dates, including periods of recruitment, exposure, follow-up, and data collection	Method, paragraph 1 and 2
Participants	6	(*a*) *Cohort study*—Give the eligibility criteria, and the sources and methods of selection of participants. Describe methods of follow-up *Case-control study*—Give the eligibility criteria, and the sources and methods of case ascertainment and control selection. Give the rationale for the choice of cases and controls *Cross-sectional study*—Give the eligibility criteria, and the sources and methods of selection of participants	Method, paragraphs 1-3
		(*b*) *Cohort study*—For matched studies, give matching criteria and number of exposed and unexposed *Case-control study*—For matched studies, give matching criteria and the number of controls per case	Not applicable
Variables	7	Clearly define all outcomes, exposures, predictors, potential confounders, and effect modifiers. Give diagnostic criteria, if applicable	S3 Table
Data sources/ measurement	8*	For each variable of interest, give sources of data and details of methods of assessment (measurement). Describe comparability of assessment methods if there is more than one group	Method, paragraphs 2-3
Bias	9	Describe any efforts to address potential sources of bias	Not applicable
Study size	10	Explain how the study size was arrived at	Method, paragraphs 1-3
Quantitative variables	11	Explain how quantitative variables were handled in the analyses. If applicable, describe which groupings were chosen and why	Method, paragraph 2
Statistical methods	12	(*a*) Describe all statistical methods, including those used to control for confounding	Method, paragraph 2 S1File Modeling

		(*b*) Describe any methods used to examine subgroups and interactions	Method, paragraph 4-6 S1 File Modeling
		(*c*) Explain how missing data were addressed	Method, paragraphs 5-6 S1 File Modeling
		(*d*) *Cohort study*—If applicable, explain how loss to follow-up was addressed *Case-control study*—If applicable, explain how matching of cases and controls was addressed *Cross-sectional study*—If applicable, describe analytical methods taking account of sampling strategy	Not applicable
		(*e*) Describe any sensitivity analyses	Not applicable
Results			
Participants	13*	(a) Report numbers of individuals at each stage of study—eg numbers potentially eligible, examined for eligibility, confirmed eligible, included in the study, completing follow-up, and analysed	Results, paragraph 1-4 S1 Table
		(b) Give reasons for non-participation at each stage	Not applicable
		(c) Consider use of a flow diagram	Not applicable
Descriptive data	14*	(a) Give characteristics of study participants (eg demographic, clinical, social) and information on exposures and potential confounders	Results, paragraph 1; S3 Table
		(b) Indicate number of participants with missing data for each variable of interest	Not applicable
		(c) *Cohort study*—Summarise follow-up time (eg, average and total amount)	Not applicable
Outcome data	15*	*Cohort study*—Report numbers of outcome events or summary measures over time	Results, paragraph 1; S2 Figure, S4 Table
		Case-control study—Report numbers in each exposure category, or summary measures of exposure	Not applicable
		Cross-sectional study—Report numbers of outcome events or summary measures	Not applicable
Main results	16	(*a*) Give unadjusted estimates and, if applicable, confounder-adjusted estimates and their precision (eg, 95% confidence interval). Make clear which confounders were adjusted for and why they were included	Not applicable
		(*b*) Report category boundaries when continuous variables were categorized	Not applicable
		(*c*) If relevant, consider translating estimates of relative risk into absolute risk for a meaningful time period	Not applicable
Other analyses	17	Report other analyses done—eg analyses of subgroups and interactions, and sensitivity analyses	Results, paragraphs1-4
Discussion			
Key results	18	Summarise key results with reference to study objectives	Discussion, paragraph 1
Limitations	19	Discuss limitations of the study, taking into account sources of potential bias or imprecision. Discuss both direction and magnitude of any potential bias	Discussion, paragraphs 2-4

Interpretation	20	Give a cautious overall interpretation of results considering objectives, limitations, multiplicity of analyses, results from similar studies, and other relevant evidence	Discussion, paragraphs 1-8
Generalisability	21	Discuss the generalisability (external validity) of the study results	Discussion, paragraph 9
Other information			
Funding	22	Give the source of funding and the role of the funders for the present study and, if applicable, for the original study on which the present article is based	Funding

*Give information separately for cases and controls in case-control studies and, if applicable, for exposed and unexposed groups in cohort and cross-sectional studies.

Note: An Explanation and Elaboration article discusses each checklist item and gives methodological background and published examples of transparent reporting. The STROBE checklist is best used in conjunction with this article (freely available on the Web sites of PLoS Medicine at http://www.plosmedicine.org/, Annals of Internal Medicine at http://www.annals.org/, and Epidemiology at http://www.epidem.com/). Information on the STROBE Initiative is available at www.strobe-statement.org.

Company	Antibody	Clone
BioLegend	Brilliant Violet 421 anti-human CD19	HIB19
	PE-Cy7 anti-human CD5	UCHT2
	Pacific Blue anti-human CD3	OKT3
	PE anti-human CD8	SK1
	PE anti-human CD69	FN50
	APC anti-human CD184	12G5
	Brilliant Violet 421 Mouse IgG1 isotype control	MOPC-21
	PE-Cy7 Mouse IgG1 isotype control	MOPC-21
	Pacific Blue Mouse IgG1 isotype control	MOPC-21
	PE Mouse IgG1 isotype control	MOPC-21
	APC Mouse IgG2a isotype control	MOPC-173
BD Biosciences	PE-Cy5 anti-human CD4	RPA-T4
	PE-Cy7 anti-human CD56	B159
	FITC anti-human CD279	MIH4
	PE-Cy7 anti-human CD25	M-A251
	FITC anti-human CD127	HIL-7R-M21
	Phosflow anti-BTK (pY223) / ITK(pY180)	N35-86
	AlexaFluor 647 anti-human BTK	53/BTK
	PE-Cy5 Mouse IgG1 isotype control	MOPC-21
	PE-Cy7 Mouse IgG1 isotype control	MOPC-21
	FITC Mouse IgG1 isotype control	MOPC-21
	PE Mouse IgG1 isotype control	MOPC-21
	AlexaFluor 647 Mouse IgG1 isotype control	MOPC-21

S1 Table: **Antibodies used in the study**

Initial nlme model	Error model	Random effects (r.e)	Correlations of r.e	Covariates
$nlme_1$	Constant	None	None	None
$nlme_2$	Constant	All	None	All parameters
$nlme_3$	Constant	μ_B, μ_4, μ_8, μ_{NK}, μ_{reg}	None	None
$nlme_4$	Constant	F_{out}, F_{in}	None	F_{in}, μ_B
$nlme_5$	B_{LN}: Constant B_{bl}, T: Proportional	All	(F_{out}, F_{in})	F_{out}, F_{in}, μ_4

S2 Table: **Initial configurations of nonlinear mixed-effect (nlme) model used with SAMBA [1].** The second column indicates which error model has been used (Constant or Proportional). The third column indicates which random effects (r.e) were accounted for. The fourth column indicates which correlations of random effects were considered. The fifth column indicates whether covariates were included, and if so on which parameters. Parameters are described in Table 1 (main text).

Reference:

[1] Prague M, Lavielle M. SAMBA: A novel method for fast automatic model building in nonlinear mixed-effects models. CPT Pharmacom & Syst Pharma. 2022 Feb;11(2):161–72.

	Cohort 1	Cohort 2	Total Cohort (1 + 2)	Total Cohort tHL group	Total Cohort pHL group
Number of patients	*41*	*81*	*122*	*68*	*54*
	Nb (%)	Nb (%)	Nb (%)	Nb (%)	Nb (%)
Sex M	27 (66%)	55 (66%)	82 (68%)	49 (72%)	33 (61%)
F	14 (34%)	26 (32%)	40 (33%)	19 (28%)	21 (39%)
Number of patients	*41*	*81*	*122*	*68*	*54*
Median age (yrs)	70	70	70	68	73
Number of patients	*41*	*81*	*122*	*68*	*54*
	Nb (%)	Nb (%)	Nb (%)	Nb (%)	Nb (%)
First Line	14 (34%)	20 (25%)	33 (27%)	21 (31%)	12 (22%)
Relapsed/Refractory	27 (66%)	61 (75%)	89 (73%)	47 (69%)	42 (78%)
Number of patients	*41*	*73*	*114*	*65*	*49*
	Nb (%)	Nb (%)	Nb (%)	Nb (%)	Nb (%)
IGHV mutational status UM	31 (76%)	56 (77%)	87 (76%)	52 (80%)	35 (71%)
M	10 (24%)	17 (23%)	27 (24%)	13 (20%)	14 (29%)
Number of patients	*40*	*75*	*115*	*66*	*49*
	Nb (%)	Nb (%)	Nb (%)	Nb (%)	Nb (%)
Del 17p	20 (50%)	26 (35%)	46 (40%)	32 (48%)	14 (29%)
Number of patients	*40*	*75*	*115*	*66*	*49*
	Nb (%)	Nb (%)	Nb (%)	Nb (%)	Nb (%)
Del 11q	15 (38%)	31 (41%)	46 (40%)	22 (33%)	24 (49%)
Number of patients	*41*	*69*	*110*	*62*	*48*
	Nb (%)	Nb (%)	Nb (%)	Nb (%)	Nb (%)
Complex karyotype	19 (46%)	26 (38%)	45 (41%)	26 (45%)	19 (40%)
Number of patients	*40*	*40*	*80*	*53*	*27*
	Nb (%)	Nb (%)	Nb (%)	Nb (%)	Nb (%)
Bulky (LN > 5cm)	5 (35%)	24 (60%)	38 (48%)	24 (45%)	14 (52%)
Number of patients	*40*	*38*	*78*	*51*	*27*
	Nb (%)	Nb (%)	Nb (%)	Nb (%)	Nb (%)
Bulky spleen	10 (25%)	18 (47%)	28 (36%)	20 (39%)	8 (30%)

S3 Table: **Clinical characteristics of patients.**
tHL: transient hyperlymphocytosis group; pHL: prolonged hyperlymphocytosis group
Nb: number; Tt: treatment; LN: Lymph Nodes

	tHL group	pHL group
Number of patients	68	54
Richter Transformation	Nb (%)	Nb (%)
All cases	**11 (16%)**	**2 (3%)**
< 1 yr of treatment	**6 (9%)**	**0 (0%)**
Progressive disease	Nb (%)	Nb (%)
All cases	17 (25%)	11 (20%)
< 1 yr of treatment	4 (6%)	2 (4%)
Total Death	Nb (%)	Nb (%)
All cases	30 (44%)	26 (48%)
< 1 yr of treatment	**10 (14.7%)**	**3 (5.5%)**
Toxicity	Nb (%)	Nb (%)
All cases	18 (26%)	12 (22%)
Lethal toxicity	9 (13%)	8 (15%)
< 1 yr of treatment	**9 (13%)**	**3 (5.5%)**
Lethal toxicity	**5 (7%)**	**0 (0%)**

S4 Table: **Clinical outcome of CLL patients according to transient hyperlymphocytosis (tHL) and prolonged hyperlymphocytosis (pHL) groups.**
Nb: number

Parameter	tHL group		pHL group		Units
	value	CI	value	CI	
F_{out}	0.0041	[0.0034;0.0048]	0.031	[0.028;0.033]	d^{-1}
F_{in}	7.76	[7.75;7.77]	3.26	[3.256;3.261]	cells.d^{-1}
μ_B	0.037	[0.036;0.038]	0.021	[0.018;0.024]	d^{-1}
μ_4	21	[17;27]	23	[18;29]	$cells^{-1}.d^{-1}$
μ_8	27	[21;33]	23	[18;29]	$cells^{-1}.d^{-1}$
μ_{NK}	70	[56;87]	56	[47;67]	$cells^{-1}.d^{-1}$
μ_{reg}	351	[267;466]	270	[215;345]	$cells^{-1}.d^{-1}$

S5 Table: **Parameter values associated with the best fit of average clinical data for both transient hyperlymphocytosis (tHL) and prolonged hyperlymphocytosis (pHL) groups and used in Figure 4C.** Parameters are described in Table 1 (main text). (CI - confidence intervals, based on the profile likelihood [1]; d – day).

Reference:

[1] Raue A, Kreutz C, Maiwald T, Bachmann J, Schilling M, Klingmüller U, et al. Structural and practical identifiability analysis of partially observed dynamical models by exploiting the profile likelihood. Bioinformatics. 2009;25: 1923–1929. doi:10.1093/bioinformatics/btp358

Parameter	Value	SD	Units
Fixed Effects			
F_{out}^t	0.001	0.0003	d^{-1}
F_{out}^p	0.044	0.009	d^{-1}
F_{in}^t	0.99	0.08	cells.d^{-1}
F_{in}^p	0.219	0.02	cells.d^{-1}
μ_B	0.023	0.0004	d^{-1}
μ_4^t	7.17	0.37	$cells^{-1}.d^{-1}$
μ_4^p	9.27	0.53	$cells^{-1}.d^{-1}$
μ_8	9.21	0.50	$cells^{-1}.d^{-1}$
μ_{NK}	35.77	2.07	$cells^{-1}.d^{-1}$
μ_{reg}	211.85	12.63	$cells^{-1}.d^{-1}$
Random Effects			
$\omega_{F_{out}}$	1.89	0.16	d^{-1}
$\omega_{F_{in}}$	1.70	0.06	cells.d^{-1}
ω_{μ_B}	0.67	0.01	d^{-1}
ω_{μ_4}	0.87	0.05	$cells^{-1}.d^{-1}$
ω_{μ_8}	0.69	0.06	$cells^{-1}.d^{-1}$
$\omega_{\mu_{NK}}$	1.0	0.04	$cells^{-1}.d^{-1}$
$\omega_{\mu_{reg}}$	0.97	0.08	$cells^{-1}.d^{-1}$
Error Parameters			
a_{BLN}	0.23	0.02	cells
b_{Bbl}	0.67	0.009	NU
b_4	0.36	0.002	NU
b_8	0.38	0.003	NU
b_{NK}	0.56	0.004	NU
b_{reg}	0.60	0.006	NU
Correlations			
$c(F_{out}, F_{in})$	-0.71	0.03	NU
$c(\mu_4, \mu_8)$	0.78	0.03	NU
$c(\mu_4, \mu_{NK})$	0.63	0.04	NU
$c(\mu_4, \mu_{reg})$	0.87	0.01	NU
$c(\mu_8, \mu_{NK})$	0.43	0.07	NU
$c(\mu_8, \mu_{reg})$	0.61	0.06	NU
$c(\mu_{NK}, \mu_{reg})$	0.75	0.02	NU
Goodness to fit			
$-2LL$	285	21	NU

S6 Table: **Parameter values associated with the best fit of individual patient measurements.** Values are averaged over 10 runs with different initial guess. Parameters are described in Table 1 (main text) and in S1 File Modeling. For fixed parameters F_{out}, F_{in} and μ_4, superscripts t and p refer to tHL (transient hyperlymphocytosis) and pHL (prolonged hyperlymphocytosis) groups, respectively, identified by a covariate (see Section 2.2 in S1 File Modeling). Coefficient $c(x, y)$ is the correlation coefficient between x and y computed by Monolix (see section 2.1 in S1 File Modeling). (SD – standard deviation; LL – log-likelihood; d – day; NU - no unit).

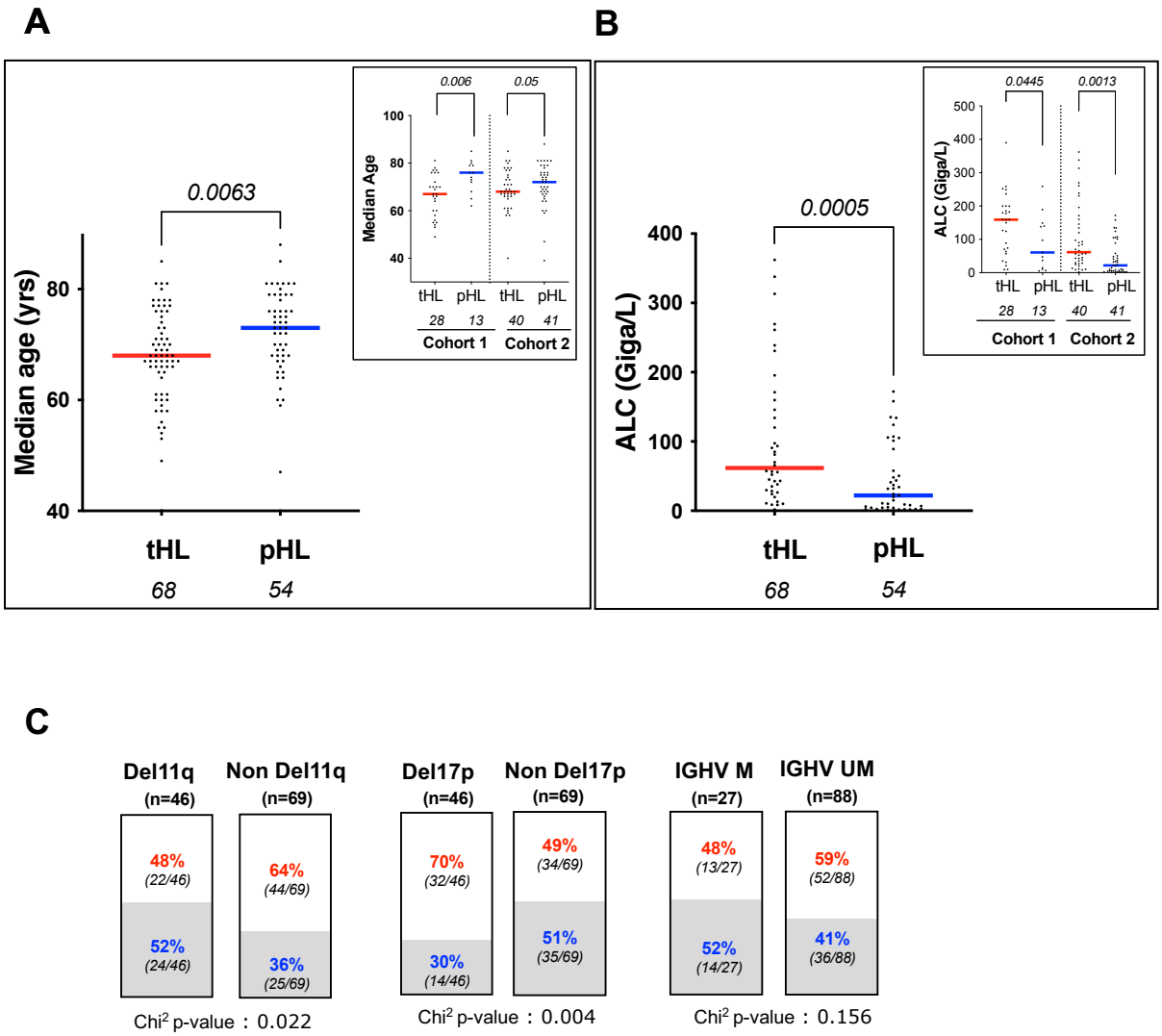

S1 Fig. **Analysis of factors associated with hyperlymphocytosis**. Median of percent change in age **(A)** and absolute lymphocyte counts (ALC) **(B)** (insert: according to cohort 1 and 2) in transient hyperlymphocytosis (tHL) and prolonged hyperlymphocytosis (pHL) groups; each dot represents a patient. **(C)** Percent of patients in tHL (red) and pHL (blue) groups according to genetic alterations. Del: deletion; IGHV M: mutated immunoglobulin heavy chain variable region genes; IGHV UM: unmutated immunoglobulin heavy chain variable region genes.

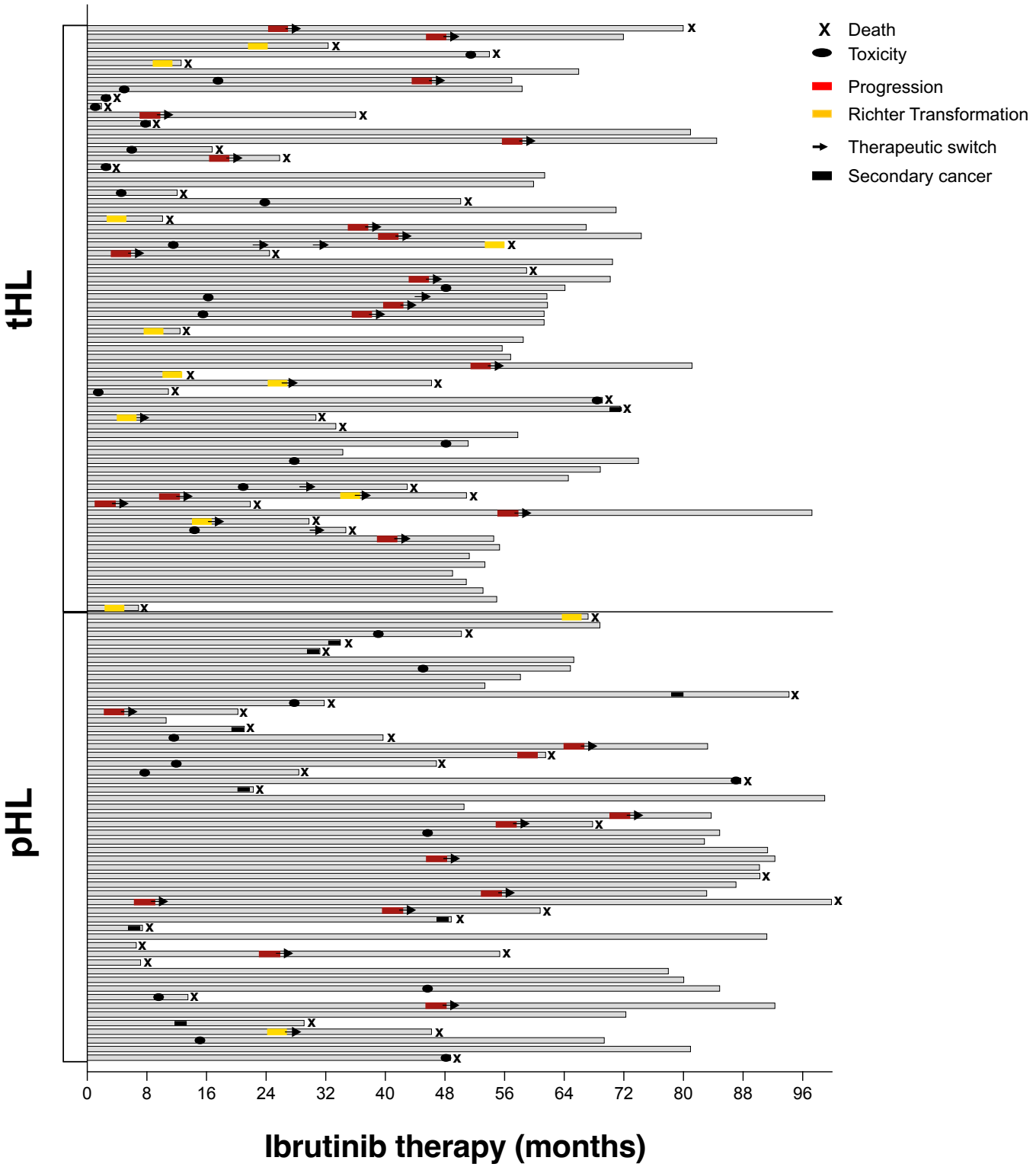

S2 Fig. **Long-term evolution of patients under ibrutinib therapy.** transient hyperlymphocytosis group (tHL) (n=68); prolonged hyperlymphocytosis group (pHL) (n=52); each line represents a patient.

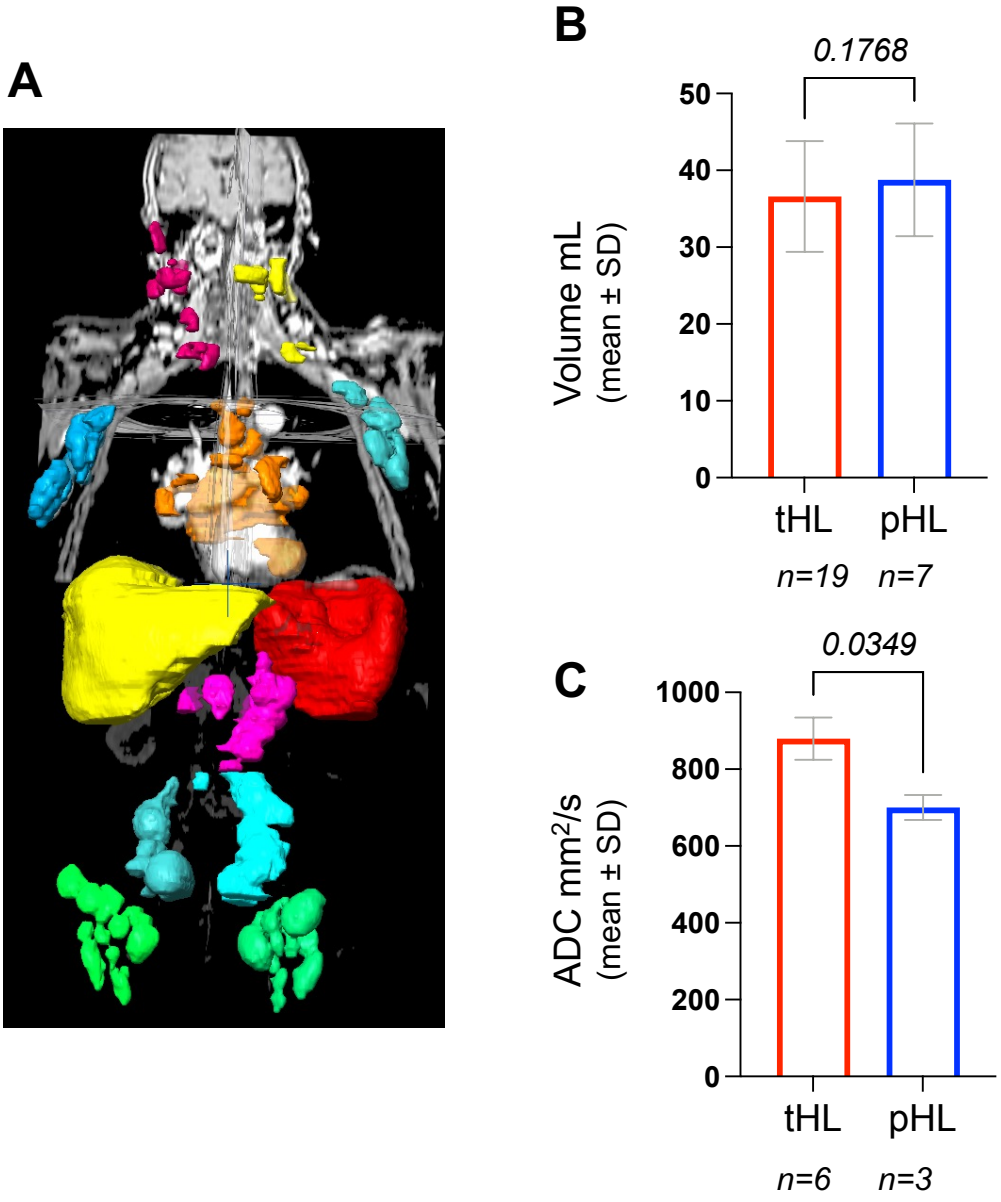

S3 Fig. **Magnetic resonance imaging (MRI) analysis before ibrutinib treatment**. **(A)** Representative features of total body MRI for a patient before ibrutinib treatment. Arbitrary colors indicate the different organs of interest (cervical, axillary, mediastinal, retroperitoneal, iliac lymph nodes, spleen and liver). **(B)** Volume of lymph nodes according to transient hyperlymphocytosis group (tHL) and prolonged hyperlymphocytosis group (pHL); **(C)** ADC of lymph nodes according to tHL and pHL groups. SD: standard deviation

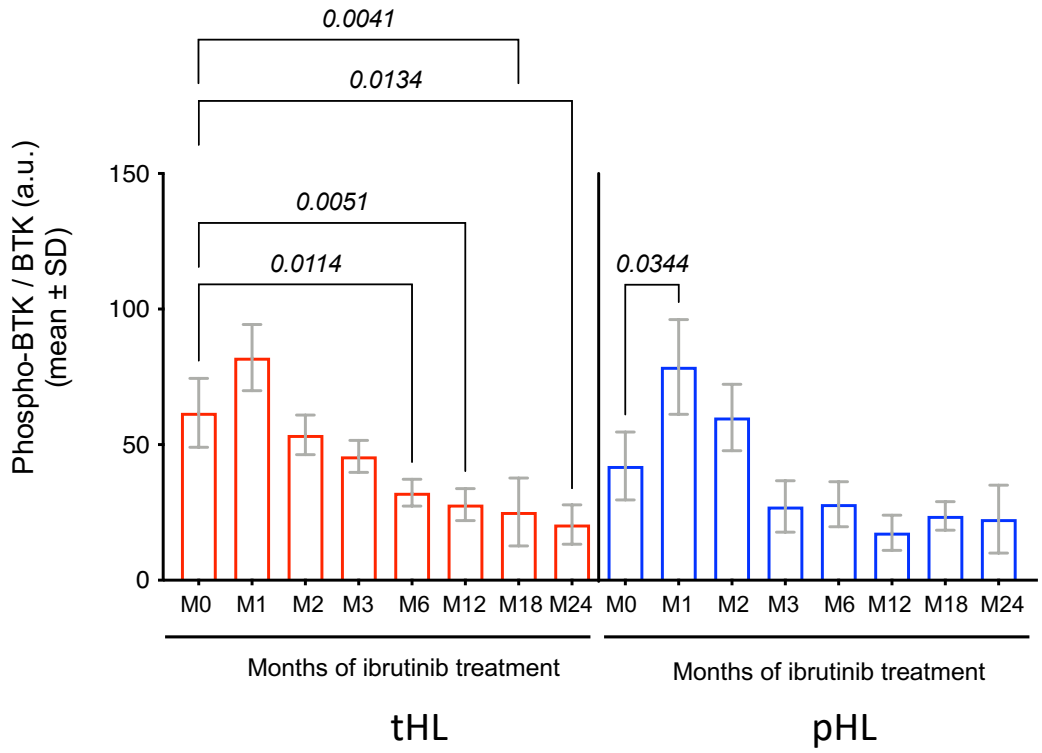

S4 Fig. **Monitoring of phosphoBTK/BTK along ibrutinib treatment**.
tHL: transient hyperlymphocytosis group; pHL: prolonged hyperlymphocytosis group.
SD: standard deviation; a.u.: arbitrary units

New pharmacodynamic parameters linked with ibrutinib responses: prospective study in real-world patients and mathematical modeling

Sarah Cadot*, Chloe Audebert*, Charlotte Dion, Soleakhena Ken, Loic Dupré, Laetitia Largeaud, Camille Laurent, Loic Ysebaert, Fabien Crauste and Anne Quillet-Mary

Supporting Information: S1 Modeling

1 Mathematical model of an average patient

1.1 Mathematical model.

In order to build a dynamical model of cells dynamics in patients treated with Ibrutinib, we account for clinical observable variables. These variables are leukemic B cell counts in lymph nodes (denoted by B_{LN}), and leukemic B cell (B_{bl}), CD4 T cell (T_4), CD8 T cell (T_8), NK cell (T_{NK}), and Regulatory CD4 T cell (T_{regs}) counts in blood.

Inspired by [9], dynamics of B cells are assumed to be described by

$$\frac{dB_{LN}}{dt} = -\mu_B B_{LN} - F_{out} B_{LN} + F_{in}, \tag{1}$$

$$\frac{dB_{bl}}{dt} = -\mu_B B_{bl} + F_{out} B_{LN}. \tag{2}$$

Leukemic B cells exit the lymph nodes (LN) with a rate F_{out}, and they are produced within LN with a constant rate F_{in}. For the sake of simplicity, the same death rate (μ_B) is assumed for leukemic B cells whether in LN or in blood.

Dynamics of T cells are assumed to follow a standard equation,

$$\frac{dT_X}{dt} = r_X(T_X, B)T_X + F_{in}^X, \tag{3}$$

where r_X is a net growth rate, incorporating cell divisions and deaths, and F_{in}^X a source term of T cells of type X exiting the LN and entering blood.

Different assumptions lead to various renewal rates: whether accounting for proliferation of T cells or not, for Tregs-mediated regulation or not, for B cell-mediated proliferation or not, for instance. Based on the ability to generate dynamics in agreement with measured cell counts, we assumed no proliferation of T cells in blood and a Tregs-mediated regulation of T cell death, that is

$$r_X(T_X, B) = -\mu_X T_{regs}. \tag{4}$$

The specificity of some dynamics observed in the cohort 1 data relies in important, and sometimes prolonged, increase of B or T cell counts in blood following the onset of the treatment. Ibrutinib is known to deplete LN of leukemic B cells, therefore it may be hypothesized that not only B but also T cells exit the LN following Ibrutinib treatment. Ideally, the source term F_{in}^X would depend on the number of T cells of type X in LN. Yet, this information is not available, only leukemic B cell counts are measured in LN. We then assumed that for each T cell population the flux of cells from the LN is proportional to the number of leukemic B cells in the lymph nodes, B_{LN}, and write

$$F_{in}^X = \alpha_{in}^X B_{LN}. \tag{5}$$

The model made of equations (1) to (5) describes the evoluton of absolute B and T cell counts in LN and blood. Since hyperlymphocytosis is defined with respect to the pre-treatment measurement ($t = \text{M0}$), we chose to focus on the evolution of normalized cell counts and rewrote the model,

$$\begin{aligned}
\frac{dB_{LN}^n}{dt} &= -\mu_B B_{LN}^n - F_{out} B_{LN}^n + F_{in} \frac{1}{B_{LN}^0}, \\
\frac{dB_{bl}^n}{dt} &= -\mu_B B_{bl}^n + F_{out} \left(\frac{B_{LN}^0}{B_{bl}^0}\right) B_{LN}^n, \\
\frac{dT_X^n}{dt} &= \alpha_{in}^X \left(\frac{B_{LN}^0}{T_X^0}\right) B_{LN}^n - \mu_X T_{regs}^0 T_{regs}^n T_X^n.
\end{aligned} \tag{6}$$

where B_{LN}^n and B_{bl}^n are the normalized cell counts of leukemic B cells in the LN and blood respectively, and T_X^n the normalized cells counts of T cells of type X. Initial cell counts measured before treatment are denoted by B_{LN}^0, B_{bl}^0 and T_X^0 for leukemic B cells in LN, in blood and for T cells. These initial counts are known from cohort 1 clinical measurements. As a consequence, initial conditions of System (6) equal 1 for all populations.

Preliminary analysis of cell count measurements highlighted a strong correlation between CD8 and CD4 T cell counts ($r^2 = 0.98$ for tHL group , $r^2 = 0.95$ for pHL group). Consequently, in the rest of the modeling part we only considered one equation – for CD4 T cells – instead of two equations for CD8 and CD4 T cell populations. Keeping in mind that there are then 3 types of T cells (CD4, NK and regulatory T cells), System (6) comprises 9 parameters: 3 parameters associated with B cell dynamics and 6 parameters associated with T cell dynamics.

1.2 Data Fitting and Quality-of-Fit Criterion.

Model (6) has been compared to data consisting in mean values of cell counts at M1, M2, M3, M6, M12, M18 and M24 for blood measurements, and M1, M12 an M24 for LN measurements. Least-squares have been used to optimize parameter values, that is the quantity

$$LS_{B_{LN}} + LS_{B_{bl}} + LS_{T_4} + LS_{T_{NK}} + LS_{T_{regs}}$$

has been minimized, where

$$LS_X = \sum_{i=1}^{n_X} \left(X(t_i) - \bar{X}_i\right)^2,$$

with $\bar{X}_i$ the mean value of observable X at time t_i. Number of measurements n_X equals 7 for all cell populations, except for leukemic B cell counts in LN where $n_{B_{LN}} = 3$ (M1, M12, M24).

Parameter value estimation and data fitting have been performed using Data2Dynamics, a Matlab R2019b add-on that allows to fit ordinary differential equation models to data and imple-ments, among other specificities, statistical assessment of parameter [6, 7].

1.3 Model selection.

Model selection was performed from the model made of equations (6). A list of models was compared to data, parameter values were estimated, and statistical indicators computed to determine which model fits data the best.

The list of models is presented in Table 1. All models are modifications of the model made of equations (6) and comprising 9 parameters. Modifications mostly lead to reduce the number of parameters to estimate (from 9 parameters for the initial model down to 5 parameters for the most simplified one). Parameter estimation is performed through the procedure in Section 1.2. In order to balance the quality of fit and the complexity of the models, statistical indicators are used to weigh the ability of a given model to appropriately fit the data. The corrected Akaike Information Criterion (AICc) is used [2]. It is the most adapted criterion here, due to the number of parameters and the quantity of data. However, for information purposes, the Bayesian Information Criterion (BIC) is also computed. It is noticeable that both AICc and BIC provide here the same conclusions.

We have to mention that the B cell model (from Wodarz et al [9]) has not been modified, because it has already been validated in the case of CLL and it very well describes B cell dynamics, in the LN and in blood, as confirmed by our numerous simulations.

We remind that

$$AICc = 2k\text{–}2LL + 2\frac{k(k+1)}{n-(k+1)},$$

with n the size of the sample (here $n = 35$), k the number of parameters, and LL the log-likelihood, and

$$BIC = \log(n)k\text{–}2LL.$$

One may note that the total number of parameters k is equal to the number of parameters of the structural model (here from 5 to 9) plus the 3 error parameters. Indeed, we assumed an error parameter for B cell counts in LN, another error parameter for B cell counts in blood, and a unique error parameter for T cell counts in blood. We performed several tests and none showed any relevance to consider an error parameter for each T cell population.

Noticeably, some models may be unidentifiable. This means that comparison of the model to data does not allow to estimate uniquely parameter values (often combinations of parameter values) that best reproduce the data. Unidentifiability is either due to a lack of information (not enough data to estimate parameter values) or to correlations in parameter values. Here the latter explanation is the reason for unidentifiability (because for most models identifiability is reached, so the problem does not come from the data). We hence indicated in Table 2 when models were identifiable ('y' for identifiable, 'n' for unidentifiable, column 6 labeled 'Ident.').

Results of model selection are presented in Table 2. Depending on the group (tHL or pHL), models fit differently the data, yet model 26 is always associated with the best AICc. This model has then been selected and used throughout the manuscript.

For the sake of clarity, it may be mentioned that other models were tested:

- Variations of models listed in Table 1 with one or more α_{in}^X coefficients equal to zero (meaning no source term for one or more T cell populations) have been compared to data but they generated either unidentifiable models or unsatisfactory models, the selection procedure highlighting that small values of parameters α_{in}^X always gave better results than no parameter α_{in}^X.

- Models accounting for proliferation of T cells (either a constant proliferation rate or a T cell mediated proliferation rate) have also been tested, but fits to data are not better and most of the time models are unidentifiable (due to a lack of information in the data that would allow to measure T cell proliferation).

Table 1: List of models tested. Models are numbered from 1 to 26, and appropriate descriptions are provided.

Model	Description
1	Model (6)
2	Model (6) with $\mu_4 = \mu_{NK}$
3	Model (6) with $\mu_4 = \mu_{NK}$ and $\alpha_{in}^4 = \alpha_{in}^{NK}$
4	Model (6) with $\mu_4 = \mu_{NK}$ and $\alpha_{in}^4 = \alpha_{in}^{reg}$
5	Model (6) with $\mu_4 = \mu_{NK}$ and $\alpha_{in}^{NK} = \alpha_{in}^{reg}$
6	Model (6) with $\mu_4 = \mu_{NK}$ and $\alpha_{in}^4 = \alpha_{in}^{NK} = \alpha_{in}^{reg}$
7	Model (6) with $\mu_4 = \mu_{reg}$
8	Model (6) with $\mu_4 = \mu_{reg}$ and $\alpha_{in}^4 = \alpha_{in}^{NK}$
9	Model (6) with $\mu_4 = \mu_{reg}$ and $\alpha_{in}^4 = \alpha_{in}^{reg}$
10	Model (6) with $\mu_4 = \mu_{reg}$ and $\alpha_{in}^{NK} = \alpha_{in}^{reg}$
11	Model (6) with $\mu_4 = \mu_{reg}$ and $\alpha_{in}^4 = \alpha_{in}^{NK} = \alpha_{in}^{reg}$
12	Model (6) with $\mu_{NK} = \mu_{reg}$
13	Model (6) with $\mu_{NK} = \mu_{reg}$ and $\alpha_{in}^4 = \alpha_{in}^{NK}$
14	Model (6) with $\mu_{NK} = \mu_{reg}$ and $\alpha_{in}^4 = \alpha_{in}^{reg}$
15	Model (6) with $\mu_{NK} = \mu_{reg}$ and $\alpha_{in}^{NK} = \alpha_{in}^{reg}$
16	Model (6) with $\mu_{NK} = \mu_{reg}$ and $\alpha_{in}^4 = \alpha_{in}^{NK} = \alpha_{in}^{reg}$
17	Model (6) with $\mu_4 = \mu_{NK} = \mu_{reg}$
18	Model (6) with $\mu_4 = \mu_{NK} = \mu_{reg}$ and $\alpha_{in}^4 = \alpha_{in}^{NK}$
19	Model (6) with $\mu_4 = \mu_{NK} = \mu_{reg}$ and $\alpha_{in}^4 = \alpha_{in}^{reg}$
20	Model (6) with $\mu_4 = \mu_{NK} = \mu_{reg}$ and $\alpha_{in}^{NK} = \alpha_{in}^{reg}$
21	Model (6) with $\mu_4 = \mu_{NK} = \mu_{reg}$ and $\alpha_{in}^4 = \alpha_{in}^{NK} = \alpha_{in}^{reg}$
22	Model (6) with $\alpha_{in}^4 = \alpha_{in}^{NK}$
23	Model (6) with $\alpha_{in}^4 = \alpha_{in}^{reg}$
24	Model (6) with $\alpha_{in}^{NK} = \alpha_{in}^{reg}$
25	Model (6) with $\alpha_{in}^4 = \alpha_{in}^{NK} = \alpha_{in}^{reg}$
26	Model (6) with $\alpha_{in}^4 = \alpha_{in}^{NK} = \alpha_{in}^{reg} = F_{out}$

Table 2: Models' ranking based on the AICc. For each group (tHL group, left; pHL group, right), models have been ranked based on their AICc values, from the lowest to the higher. Unidentifiable models are ranked after all identifiable models. Column1: model's number; Column 2: number of parameters (par.); Column 3: value of -2 the log-likelihood ($-2LL$); Column 4: AICc value; Column 5: BIC value; Column 6: indicates whether the model is identifiable (y - yes; n - no).

tHL group						**pHL group**					
Model	par.	$-2LL$	AICc	BIC	Ident.	Model	par.	$-2LL$	AICc	BIC	Ident.
26	6	−131	−106	−99	y	26	6	−27	−2	5	y
17	7	−134	−105	−98	y	4	7	−26	3	10	y
10	7	−132	−103	−96	y	5	7	−26	3	10	y
5	7	−131	−102	−95	y	10	7	−26	3	10	y
8	7	−131	−102	−95	y	13	7	−26	3	10	y
12	8	−135	−102	−96	y	14	7	−26	3	10	y
2	8	−134	−101	−95	y	25	7	−26	3	10	y
4	7	−130	−101	−94	y	23	8	−25	8	14	y
13	7	−130	−101	−94	y	24	8	−25	8	14	y
25	7	−130	−101	−94	y	19	6	−0	25	32	y
7	8	−132	−99	−93	y	9	7	−2	27	34	y
22	8	−130	−97	−91	y	6	6	7	32	39	y
1	9	−134	−96	−91	y	11	6	7	32	39	y
18	6	−111	−86	−79	y	21	5	16	38	44	y
6	6	−108	−83	−76	y	20	6	16	41	48	y
3	7	−110	−81	−74	y	15	7	17	46	53	y
9	7	−107	−78	−71	y	1	9	−24	-	-	n
21	5	−100	−77	−73	y	2	8	−25	-	-	n
11	6	−104	-	-	n	3	7	−7	-	-	n
14	7	−130	-	-	n	7	8	−25	-	-	n
15	7	−104	-	-	n	8	7	−26	-	-	n
16	6	−99	-	-	n	12	8	−25	-	-	n
19	6	−107	-	-	n	16	6	17	-	-	n
20	6	−99	-	-	n	17	7	−26	-	-	n
23	8	−130	-	-	n	18	6	−8	-	-	n
24	8	−131	-	-	n	22	8	−25	-	-	n

- Finally, models that do not consider regulation of T cell dynamics by Tregs have also been considered, but they result in poor reproduction of T cell dynamics.

2 Population approach and inter-patient variability

After validating a model of B and T cell dynamics under Ibrutinib treatment for an average patient, we modified the model to account for inter-patient variability. To do so, we used a population approach based on mixed-effect modeling [4].

2.1 Nonlinear mixed-effect models

Nonlinear mixed effects models allow the description of inter-patient variability within a population of individuals. All individuals belong to the same population (here a population of LLC patients) so they share common characteristics. These are called "fixed effects" and characterize an average behavior of the population. Nevertheless, each patient is unique and differs from the average behavior by a specific value called "random effect". Details on the method can be found in [1, 3, 4, 8], we here describe only the part relevant to this study, focusing on our hypotheses.

Data $\{d_{i,j},\, i = 1, ..., N_{ind},\, j = 1, ..., n_i\}$ is assumed to satisfy

$$d_{i,j} = f(y_{i,j}, \psi_i) + (a + bf(y_{i,j}, \psi_i))\varepsilon_{i,j},$$

where $d_{i,j}$ is the j-th observation of patient i, N_{ind} is the number of patients within the population and n_i is the number of observations for the i-th patient.

The function f accounts for individual dynamics generated by a mathematical model. In this work f is associated with the solution of a system of ODE, see Section 1.1. The function f depends on known variables, denoted by $y_{i,j}$ ($e.g$ $B^0_{LN,i}$, the initial ($j = 0$) count of leukemic B cells in LN for patient i), and parameters of the i-th patient, denoted by ψ_i.

Patient-specific parameter vector ψ_i is assumed to be split into fixed effects (population-dependent effects, average behavior) and random effects (patient-dependent effects). In addition, parameters ψ_i are assumed to follow a log-normal distribution to ensure their positivity. If ψ_i^k denotes the k-th parameter characterizing patient i, then it is assumed that

$$\log(\psi_i^k) = \log(p_{pop}^k) + \eta_i^k,$$

where the vector of parameters $p_{pop} = (p_{pop}^k)_k$ models the average behavior of the population, and $\eta_i = (\eta_i^k)_k$ represents how patient i differs from this average behavior. Random effects follow a normal distribution : $(\eta_i^k)_k \sim \mathcal{N}(0, \Omega)$. Ω is the variance-covariance matrix defining the distribution of the vector of random effects. When no correlation between random effects is considered, Ω is a diagonal matrix with coefficients ω_k^2 in the diagonal. The coefficients ω_k^2 quantify the variability of the k-th parameter within the population. When a correlation between random effects is considered, the variance-covariance matrix Ω is a block diagonal matrix, with $\Omega_{i,j} = \Omega_{j,i} = c(\eta_i, \eta_j)\omega_i\omega_j$, where $c(\eta_i, \eta_j)$ is the correlation coefficient between random effects η_i and η_j.

The residual errors, combining model approximations and measurement noise, are denoted by $(a + bf)\varepsilon_{i,j}$. They quantify how the model prediction is close to the observation. Residual errors are assumed independent, identically and normally distributed, $i.e$ $\varepsilon_{i,j} \sim \mathcal{N}(0, 1)$. Moreover, the random effects η_i and the residual errors $(a + bf)\varepsilon_{i,j}$ are mutually independent.

2.2 Parameter estimation

Parameter values are estimated with Stochastic Approximation Expectation-Maximization (SAEM) algorithm. The SAEM algorithm is available in [5].

2.2.1 Population and patient-specific parameters.

Under the previous assumptions, cell population dynamics (average behavior and inter-patient variability) are described by parameters: p_{pop}, Ω, and a or b. These parameters are estimated by likelihood maximization with the SAEM algorithm.

Once these parameters have been estimated, each patient-specific vector of parameters ψ_i is estimated by maximizing the conditional probabilities

$$\mathbb{P}(\psi_i | d_{i,j}; \hat{p}_{pop}, \hat{\Omega}, \hat{a}, \hat{b}),$$

where $\hat{x}$ denotes the estimated value of x.

2.2.2 Covariates.

In order to characterize patients from tHL and pHL groups, we used categorical covariates. To do so, data of tHL and pHL groups have been pooled together, then parameter values have been estimated (see paragraph above) by assuming that fixed effects parameters of patients from pHL group were different from fixed effects parameters of tHL group patients.

Categorical covariates were introduced as follows: if a patient is either in tHL or pHL group, we assume that the probability distribution of their patient-specific parameter vector ψ_i has a different mean. We write

$$\log(\psi_i^k) = \log(p_{pop}^k) + \beta^k c_i + \eta_i^k,$$

where c_i equals 1 if patient i is in pHL group, and 0 if patient i is in tHL group, and $\beta = (\beta^k)_k$ is a vector of covariate parameters. Estimated covariate parameters $\hat{\beta}$ have been tested to be significantly different from zero with a Wald test implemented in Monolix software [5], with a p-value threshold at 0.05.

Patient dynamics are then characterized by parameters $(p_{pop}, \Omega, a, b, \beta)$. If the estimated vector $\hat{\beta}$ is significantly different from zero, then the classification in tHL or pHL groups partly explains the observed variability.

References

[1] Delyon B, Lavielle M, Moulines E (1999) Convergence of a stochastic approximation version of the EM algorithm. The Annals of Stat 27(1), 94–128.

[2] Hurvich CM and Tsai C-L (1989) Regression and time series model selection in small samples. Biometrika 76, 297—307.

[3] Kuhn E, Lavielle M (2005) Maximum likelihood estimation in nonlinear mixed effects models. Computational Statistics and Data Analysis 49(4), 1020–1038.

[4] Lavielle M (2014) Mixed effects models for the population approach. Models, Tasks, Methods and Tools. Chapmann and Hall/CRC , 383p.

[5] Monolix version 2019R1. Antony, France: Lixoft SAS, 2019.

[6] Raue A., et al. (2015) Data2Dynamics: a modeling environment tailored to parameter estimation in dynamical systems. Bioinformatics, 31(21), 3558-3560.

[7] Raue A., et al. (2013) Lessons Learned from Quantitative Dynamical Modeling in Systems Biology. PLOS ONE, 8(9), e74335.

[8] Samson A, Donnet S (2007) Estimation of parameters in incomplete data models defined by dynamical systems. Journal of Statistical Planning and Inference 137 (9), 2815–2831.

[9] Wodarz D, Garg N, Komarova NL, Benjamini O, Keating MJ, Wierda WG, Kantarjian H, James D, O'Brien S, Burger JA (2014) Kinetics of CLL cells in tissues and blood during therapy with the BTK inhibitor ibrutinib. Blood 123(26), 4132–4135.